AD-A084 400 SCIENCE APPLICATIONS INC TUCSON AZ F/G 17/4
RADAR TEST RANGE DESIGN CONSIDERATIONS.(U)
APR 80 D SOFIANOS F33657-79-C-0178
UNCLASSIFIED SAI-TR-04-165-3 NL

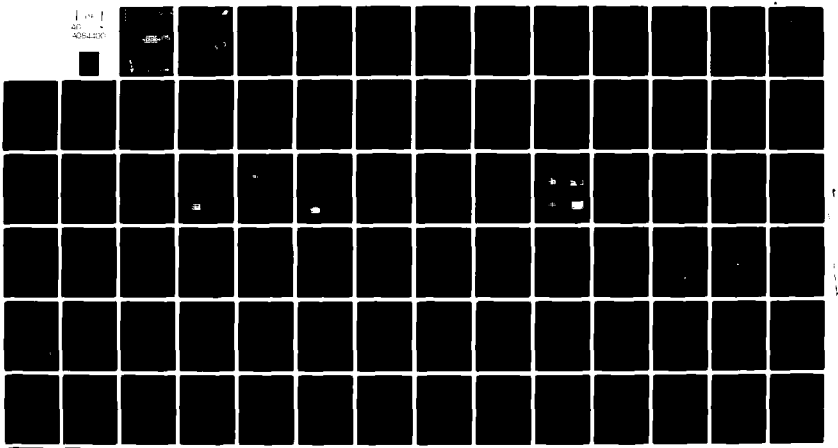

END
DATE FILMED
6-80
DTIC

(10)

LEVEL II

(10)

(6) RADAR TEST RANGE DESIGN CONSIDERATIONS,

(14) SAI-TR-04-165-3

(9) Final rept.,

Prepared for

USAF SYSTEMS COMMAND
Aeronautical System Division
UPD-X Program Office

Prepared by
(10) Dino/Sofianos

(12) 83

(11) 29 APR 1980

(15) Contract F33657-79-C-0178

CDRL 1008

Project 1-125-04-165

LPN SAI

JCB

Science Applications, Inc. 5055 E. Broadway, Suite A214 / Tucson, Arizona 85711 / (602) 748-7400

ACKNOWLEDGEMENTS

The author would like to express his appreciation to John Scott, Jerry S. Zelenka and Norman G. Massey for their aid in the development of this report.

TABLE OF CONTENTS

LIST OF TABLES

LIST OF FIGURES

1.0 INTRODUCTION

The purpose ~~of this report~~ is to present a methodology and conceptual design for a Flexible Test Bed (FTB) digital processor operational test.

The objectives of this operational test are to:

- Determine whether the processor modifications improved image quality,
- Establish a processor performance baseline,
- Determine whether the system will attain desired levels of probability of detection.

It is assumed ~~in preparing~~ this report that SAI would develop a test design while GAC will fabricate and install the required radar test range. The testing will be a joint AF/GAC effort with SAI assistance in interpreting the test data.

This report is organized as follows:

- Section 2.0 describes the basic philosophy of radar test ranges, and the characteristics of typical test site components.
- Section 3.0 defines measures of image quality and states the FTB specification.
- Section 4.0 defines the test methodology for the measurement of the FTB image quality parameters.
- Section 5.0 outlines the type and size of reflectors required to make up the test site along with practical considerations.

- Section 6.0 summarizes the test site recommendations and the priority as to which image quality measurements should be measured.

2.0 TEST PHILOSOPHY

This section will describe a philosophy of processor testing and describe some of the required test components.

2.1 General

The basic approach to testing is illustrated in Fig. 2-1. A controlled test range is imaged by the radar system flying a prescribed flight path. Image data can be measured at the three points depicted in Fig. 2-1, namely, (A) the processor output, (B) the display control output, and (C) the image. The measurement of image parameters at these three points can be compared with ground truth data to estimate the image quality being achieved with the entire system (i.e., from radar collection through image display).

This overall process involves 3 basic components which are:

- Radar Test Range
- Output Data Collection
- Comparison and Processing

Each of these is discussed in the following sections.

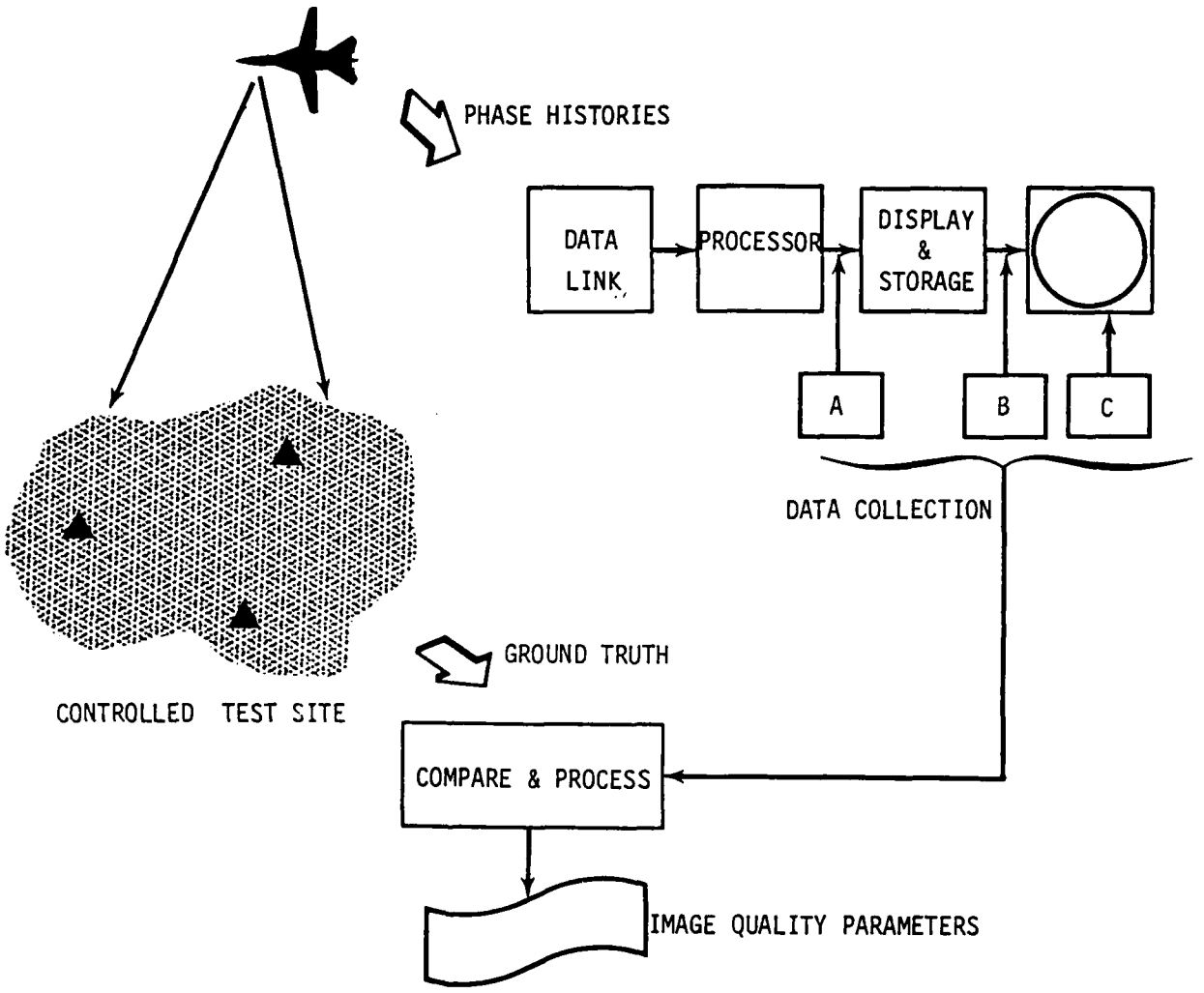

Figure 2-1. Processor Testing Using Controlled Radar Range.

2.2 Test Range Components

Two basic types of test site components are reviewed for system verification. The first type are point targets or specular reflectors and the second type are extended targets. Ten types of point targets will be considered ranging from flat plate reflectors to Luneberg lens. Examples of extended targets are bodies of water, road patterns , and terrain. Operational targets will also be considered for the verification of the FTB processor.

2.2.1 Point Targets

The point targets (specular reflectors) considered for use in the verification of the FTB processor are listed in Table 2-1. Also, listed as a function of reflector type is the maximum achievable radar cross section area, σ_{max}, and the approximate angular coverage. In Appendix A the analytical expressions for the radar cross-section as a function of look angle are presented.

In deriving σ_{max} for each of the reflector types, the following simplifying assumptions were made. First, the calculation of σ_{max} is only valid in the high frequency limit (λ << object dimensions) since they were obtained using physical optics techniques. However, these expressions, for σ_{max} are reasonably good for physical dimensions as small as 3λ since the edge effects are then neglibigly small. Secondly, the effects of sagging and warping of the surface edges is ignored. This degradation in performance is largely due to thermal expansion effects. The misalignment of the reflectors is also ignored in the computation of σ_{max}. The degradation in performance for corner reflectors is analyzed as a function of their misalignment in Appendix B. By approximating the deleterious effects

TABLE 2-1

RADAR CROSS SECTIONS OF VARIOUS RADAR REFLECTORS

REFLECTOR TYPE	σ_{max}	APPROXIMATE ANGULAR COVERAGE
1. Flat Plate	$\frac{4\pi W^2 L^2}{\lambda^2}$	$\frac{\lambda}{W} \times \frac{\lambda}{L}$
2. Finite Circular Cylinder	$\frac{\pi d L^2}{\lambda}$	$\frac{\lambda}{L} \times 2\pi$
3. Sphere	$\frac{\pi}{4} d^2$	omnidirectional
4. Dihedral Corner	$\frac{8\pi W^2 L^2}{\lambda^2}$	$\frac{\lambda}{L} \times \frac{\pi}{6}$
5. Triangular Trihedral Corner	$\frac{4\pi L^2}{3\lambda^2}$	40^0 cone about axis of symmetry
6. Square Trihedral Corner	$\frac{12\pi L^4}{\lambda^2}$	23^0 cone about axis of symmetry
7. Circular Trihedral Corner	$\frac{15.6 L^4}{\lambda^2}$	32^0 cone about axis of symmetry
8. Biconical	$\frac{4\pi}{9\lambda}\left[(d)^{3/2} - (d)^{3/2}\right]^2$	$\pm 20^0 \times 360^0$
9. Top Hat	$\frac{4\pi d L^2}{\lambda}$	$\sin\theta \times 2\pi$
10. Luneberg Lens	$\frac{\pi^3 d^4}{\lambda^2}$	130^0 cone about axis of symmetry

---

W -- width of a flat surface element

L -- length of a flat surface element or cylinder

d -- diameter

λ -- wavelength

of sagging and warping of the reflectors as a misalignment, a bound can be set on the tolerable limits for acceptable performance.

Let us now consider what practical values of σ_{max} can be achieved with the reflector types listed in Table 2-1. Two basic constraints will be imposed when considering the practical values of σ_{max}. First, the minimum dimensions of any reflector must be larger than 3λ. Second, the maximum dimensions of any reflectors have a practical limitation, which is assumed to be 6.5 ft. Since the top hat reflector has the added complication of requiring a ground plane, its maximum size is restricted to 5 ft. The construction of Luneberg lenses with diameters in excess of 3 feet appears to be prohibitively expensive, therefore a 3-foot limitation will be imposed upon them.

Using the above constraints and assuming a nominal wavelength of 0.1 ft. ,we obtain the practical ranges of σ_{max} listed in Table 2-2. As noted in Table 2-2, σ values can range from 0.07 ft^2 for a sphere to 6.7×10^6 ft^2 for a square trihedral corner. Also note that for the most common reflector type, the traingular trihedral corner, the range of σ spans from 3.3 ft^2 to 7.5×10^5 ft^2.

In Appendix B, Table B-2, the effects of corner reflector misalignments are tabulated for the triangular trihedral, square trihedral and the square dihedral. For these corner reflector types the alignment accuracies required to keep the σ_{max} losses to less than 1dB and 3dB are also presented. As an example, if a traingular trihedral reflector has a corner of one surface at the vertex displaced by $\lambda/2.6$, a 3dB loss in σ_{max} results. For a loss of less than 1dB the corresponding displacement must be less than $\lambda/4.6$. Under the same circumstances, a square trihedral

TABLE 2 - 2

AVAILABLE RADAR CROSS SECTION AS A FUNCTION OF REFLECTOR TYPE

1.	Flat Plate	$3\lambda \leq (W,L) \leq 6.5$ ft.	$10 \leq \sigma \leq 2.2 \times 10^6$
2.	Finite Circular Cylinder	$3\lambda < (d,L) \leq 6.5$ ft.	$0.8 \leq \sigma \leq 8600$
3.	Sphere	$3\lambda \leq d \leq 6.5$ ft.	$0.07 \leq \sigma \leq 33$
4.	Dihedral Corner	$3\lambda \leq (W,L) \leq 6.5$ ft.	$20 \leq \sigma \leq 4.5 \times 10^6$
5.	Triangular Trihedral Corner	$3\lambda \leq L \leq 6.5$ ft.	$3.3 \leq \sigma \leq 7.5 \times 10^5$
6.	Square Trihedral Corner	$3\lambda \leq L \leq 6.5$ ft.	$30 \leq \sigma \leq 6.7 \times 10^6$
7.	Circular Trihedral Corner	$3\lambda \leq L \leq 6.5$ ft.	$13 \leq \sigma \leq 2.8 \times 10^6$
8.	Biconical	$3\lambda < (d_1,d_2) \leq 6.5$ ft.	$0.4 \leq \sigma \leq 3800$
9.	Top Hat	$3\lambda \leq (d,L) \leq 5$ ft.	$3.3 \leq \sigma \leq 16,000$
10.	Luneberg Lens	$3\lambda \leq d \leq 3$ ft.	$6 \leq \sigma \leq 63,000$

reflector will experience a 1dB (3dB) loss if the corresponding displacement is $\lambda/8$ ($\lambda/4.5$). Therefore, the square trihedral reflector is almost twice as sensitive to reflector misalignments than the triangular trihedral corner reflector.

Using the results presented in Appendix B, we can determine how the radar cross-section σ of a triangular trihedral reflector depends upon the misalignment of one or more surfaces. In Fig. 2-2 we show how σ varies with the misalignment of one surface about it's long edge. In Fig. 2-3, we repeat the above exercise where one surface has been rotated about its short edge. Comparing the two figures, the reader will note that the triangular trihedral radar cross-section losses for the surface rotations about a short edge are almost twice as large as for those about it's misalignment along a long edge.

2.3 Extended Test Target

The extended test targets of interest include uniform ground clutter (e.g., desert, forest, ocean), man-made structures (e.g., bridges, buildings), and ground painting (e.g., cultivated field, suburban areas).

The radar reflectivity of extended test targets is usually given in terms of its backscatter coefficient σ_0, the average radar cross section per unit area. The backscatter coefficient is given for a wide range of extended test targets in Fig. 2-4. The backscatter coefficient varies from σ_0 = -40dB for a calm sea to σ_0 = +18dB for an industrial area. The test sites under consideration, Gila Bend and Ft. Huachuca, are a mixture of arid desert and broken desert for which the backscatter coefficient is expected to be between -25dB and -15dB.

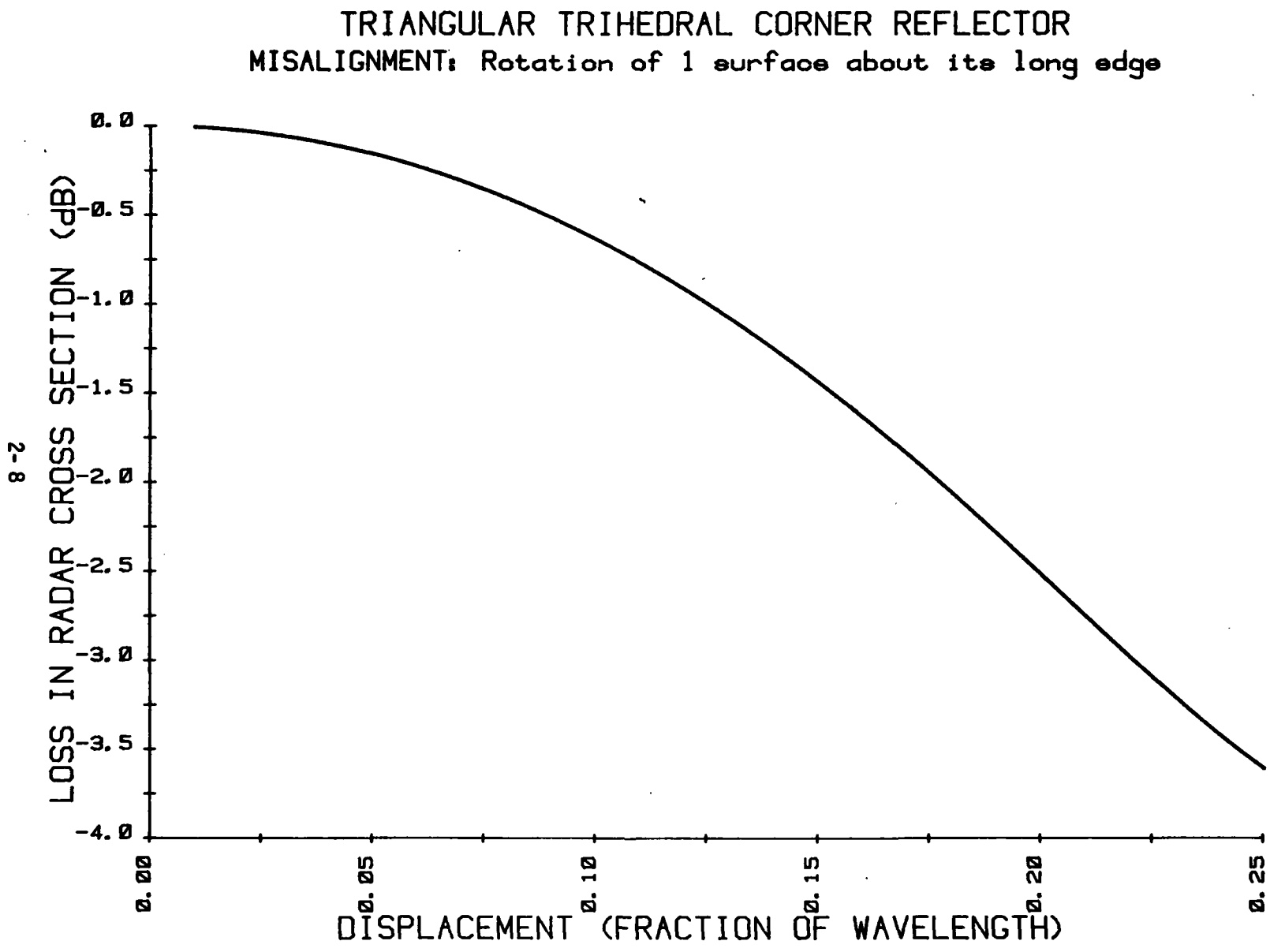

Figure 2-2. Loss in Radar Cross Section as a Function of Misalignment Error.

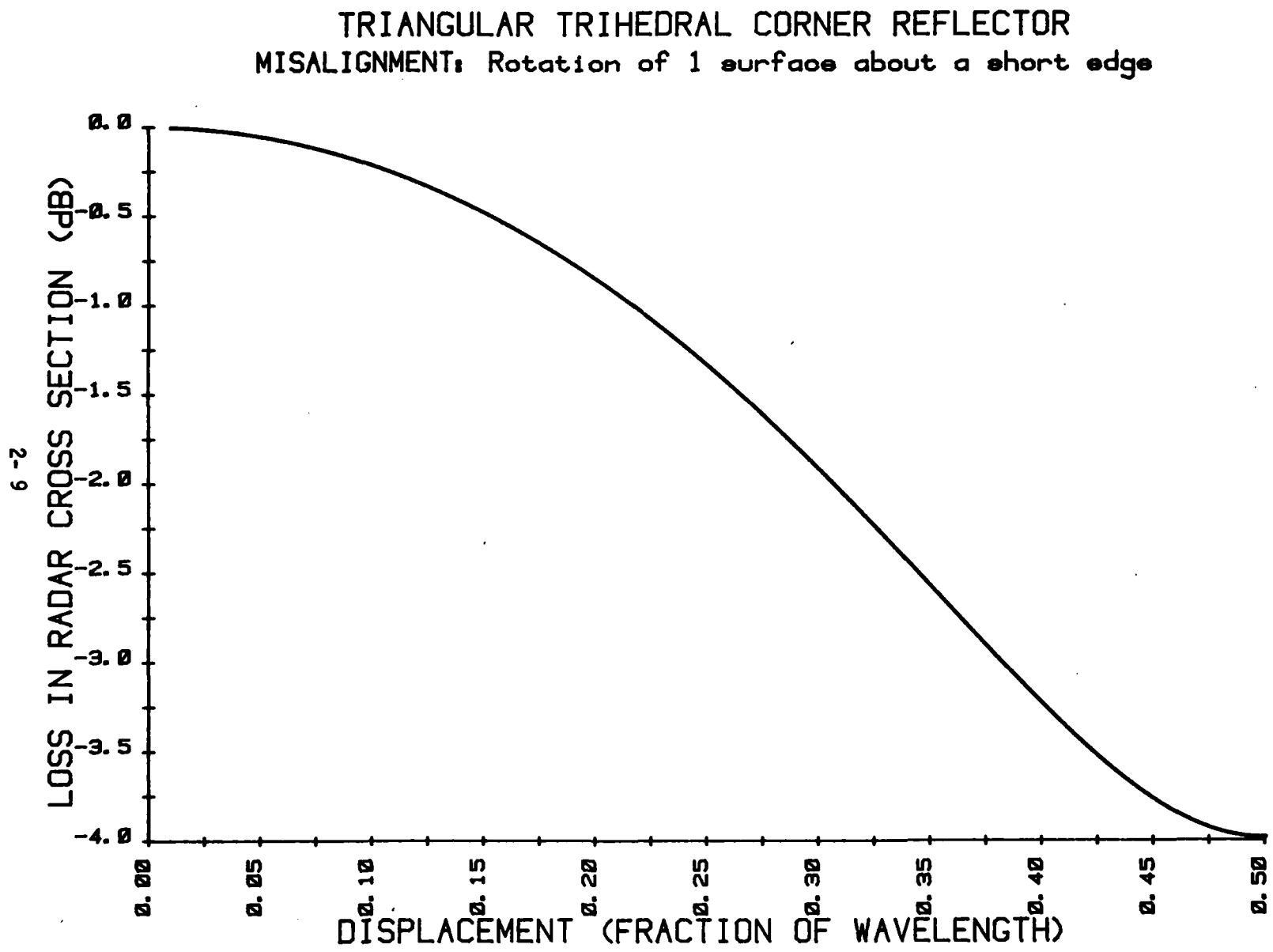

Figure 2-3. Loss in Radar Cross Section as a Function of Misalignment Error.

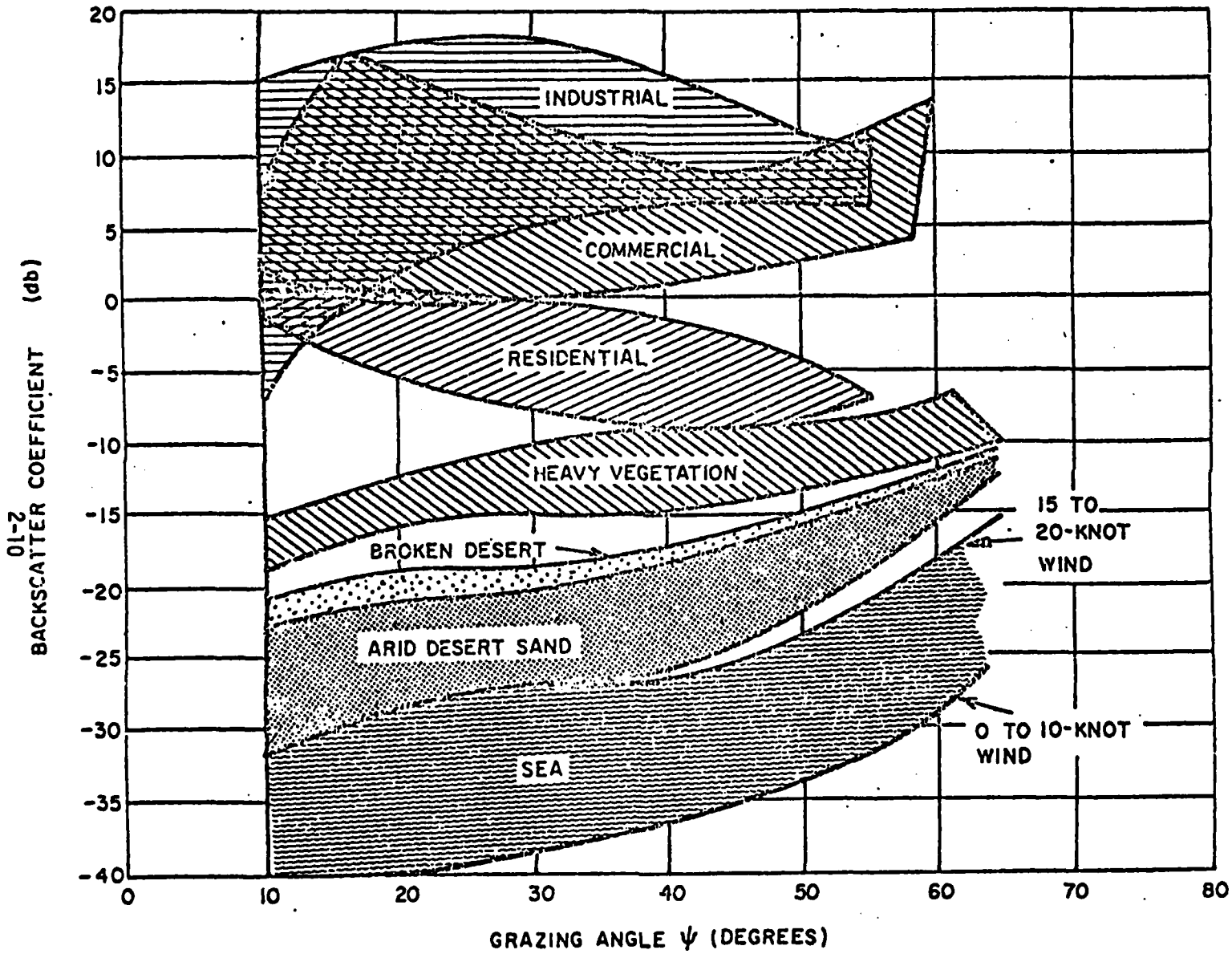

Figure 2-4. Backscatter Coefficients for Extended Targets at $\lambda \approx 0.1$ ft.

The σ_0 values associated with extended test targets are of considerable interest in determining the radar sensitivity and dynamic range requirements. However, they usually are not used to make quantitative measurements of the radar system parameters due to the wide variability of σ_0. In addition, the actual σ_0 values for extended targets are highly dependent upon meteorological and seasonal conditions.

2.4 Targets of Operational Interest

The major objective of the FTB system is the detection of operational targets. As such, this section is included to outline target sizes of interest such as jeeps, tanks, armoured personnel carriers (APC's), and trucks. From previous studies Hughes Aerospace Company (HAC) has tabulated the cross sectional areas, σ_0, of each of the aforementioned operational targets. The mean, median and variance levels of each of these targets is illustrated in Fig. 2-5. Note the wide variability of each target's cross sectional area. For the APC's the median level is $\sigma_0 = 100m^2$, yet the minimum σ_0 is $20m^2$ and it's maximum σ_0 value is $8{,}000m^2$.

Although these targets are of operational interest, due to the wide variability of their target cross sectional area it is not advisable to use them as test targets. They are included in this report only to define the relative range of σ_0 for operational targets.

TARGET RADAR CROSS SECTION (RCS) SURVEY (DEPRESSION ANGLE >5 DEGREES)

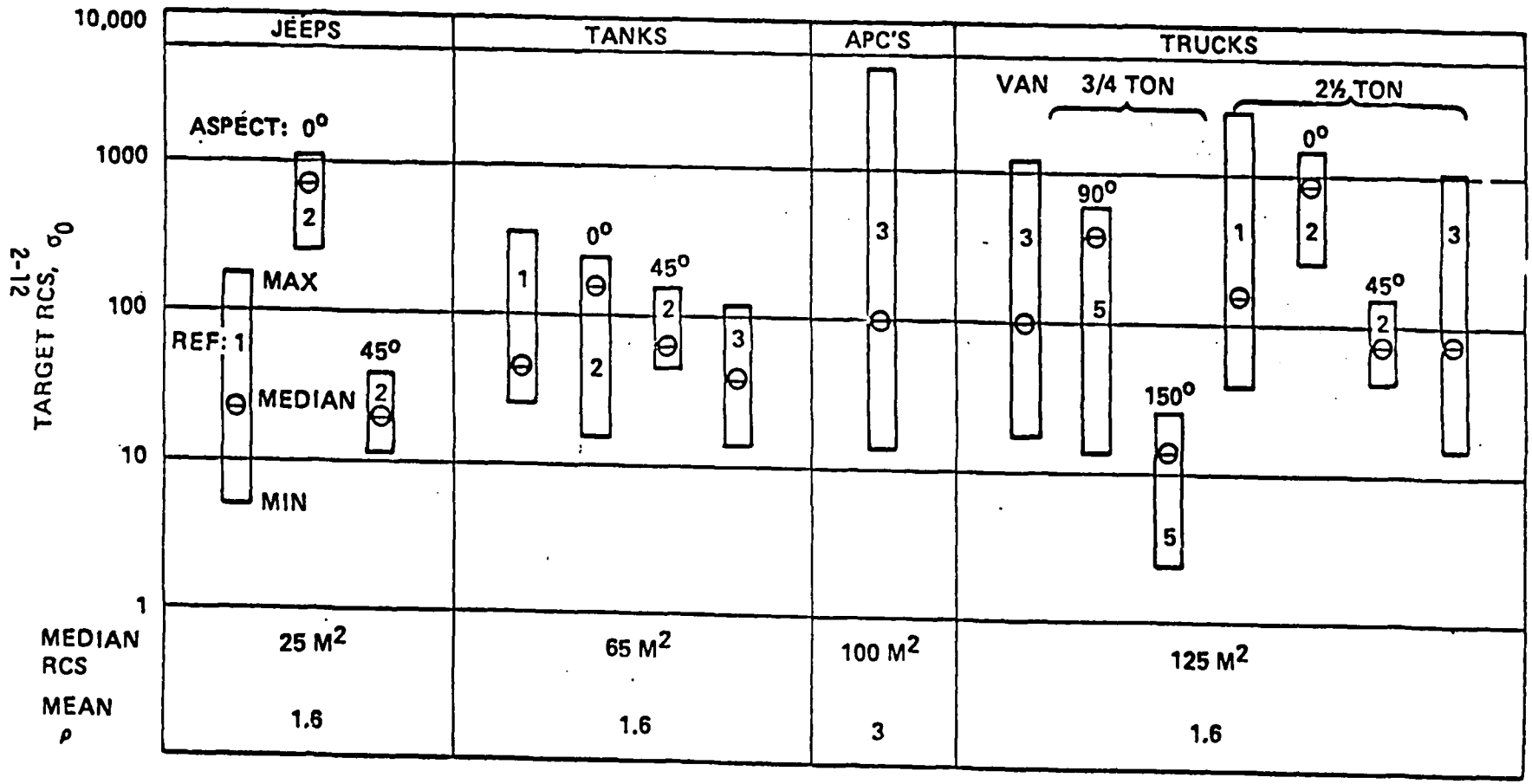

Figure 2-5.

2.5 Output Data Collection

The objective of the data collection process is to estimate image quality parameters associated with the radar processor output image. There are several ways this can be done for the FTB, three of which are illustrated in Fig. 2-1 and discussed here.

The best system indication is obtained by examining the displayed image (point C). However, this approach has several drawbacks. First, it is difficult to make accurate measurements from the screen of a CRT, which is the primary output of the FTB. Second, there are several additional processing steps between the processor and the display which distort the image in a perhaps unknown way (i.e., bit errors, decreased signal-to-noise level, loss of dynamic range, etc.).

Some of the above problems are overcome by using the image data being applied to the CRT at the output of the scan convertor (point B). At this point, it is possible to make quantitative measurements, but the effects of intermediate processing are still present.

The third measurement point is at the processor output (point A) where it is possible to make quantitative measurements of the processor output. At this point there is still the problem of distortions due to the data link, but these may be treated as part of the processing problem.

2.6 Data Processing

The processing required to compute the image quality measures is relatively straightforward and can be done either manually or with computer assistance. The choice is largely dependent on the number of times that the tests will be run and the format of the collected data.

2.6.1 Manual Processing

Any of the collection processes mentioned in paragraph 2.5 can support a manual data reduction. In each case, the image data is reduced to a group of pixel intensities from which the analyst develops image quality measures. Manual processing has the advantages of being easy and quick to implement and permitting insights into processor performance to be inferred from raw data. The disadvantages of manual processing are that it is slow, error prone, non-repeatable and of fixed cost per analysis.

2.6.2 Automatic Processing

Data collected at the processor output (point A) and scan converter output (point B) are digital and thus easily introduced into a digital computer for processing. The data obtained from the CRT is not as easily processed however, and it is best handled manually.

Goodyear Aerospace Corporation (GAC) has developed a computer program[1] for radar image quality measurement using a calibrated test range. Briefly, the GAC program utilizes digitized imagery and a knowledge of test range characteristics, such as target location and size, to produce measures of the following parameters:

- IPR
- Peak Sidelobe Level
- Linear Dynamic Range
- Intermodulation Distortion
- Position Accuracy

The program was developed for another radar system and would require modification to process the FTB data.

---

[1] - As per telephone conversation between John Scott (SAI/Tucson) and Bob Bowden (GAC/Goodyear) on February 18, 1980.

The advantages of automatic processing are that it provides fast results, it is repeatable and cheaper for multiple tests. The disadvantages are that the initial cost is high and it is not immediately available.

2.7 Summary

This section has described some of the basic issues and techniques of the FTB testing approach. The sections which follow will develop details and make recommendations on the particular test range components and layout. It will be assumed that data will be collected at the processor output (point A) and manually reduced.

3.0 FTB IMAGE QUALITY PARAMETERS

The performance parameters for the Flexible Test Bed (FTB) processor were defined during Goodyear's FTB Final Design Review (1979) and are outlined in Table 3-1. The first three entries in Table 3-1 define the basic geometry requirements. Note that the minimum operating range is 2.5 N.Mi. and the maximum operating range is 30 N.Mi. The remaining performance parameters define the image quality requirements of the system.

Let us briefly review the five image quality requirements that are given in Table 3-1.

3.1 3dB Impulse Response

The 3dB impulse response (IPR) in range and azimuth (cross range) is a measure of system resolution. Experience gained from previous programs indicate that this image quality parameter is very significant when one is attempting to do target classification and identification; image quality ratings (image interpreter scores) tend to improve as resolution (IPR width) is improved. This leads directly to improved probability of detection (P_d), a significant system goal. However, image resolution is a two-dimensional quantity and should be considered as such. The 3dB contour level (which is the area enclosed by a contour 3dB down from the peak value) associated with the impulse response of the imaging system tends to be a more appropriate measure of system resolution. Some experiments have been conducted which show that system performance does not change appreciably if the 3dB impulse response is increased somewhat in one direction and decreased in the other providing that the area defined by the 3dB contour levels remains unchanged.

TABLE 3-1

FTB PROCESSOR PERFORMANCE REQUIREMENTS[1]

Performance Parameter	Requirement
Minimum Ground Range	2.5 N.Mi.
Maximum Ground Range	30.0 N.Mi.
Slant Range Coverage (at best range IPR)	5.0 N.Mi.
Squint Angle Capability	None
Pixel Spacing (best)	15.0 ft.
IPR Width (best)	20.0 ft.
Peak Sidelobe Level	-12dB*
Linear Dynamic Range	32dB*
Image Position Accuracy	NA

[1] - Excerpted from Goodyear FTB Final Design Review, 1979.

* - Estimated

NA - not available

3.2 Peak Sidelobe Levels

Peak sidelobe levels must be under reasonable control to ensure that images of weak targets (i.e., small return areas) will not be masked by the sidelobe associated with a strong target (i.e., a bright specular return). This sidelobe requirement is especially important when one wishes to define a shadow near a bright specular target, such as, the shadow of a military vehicle situated in a weak clutter background.

3.3 Linear Dynamic Range

A large linear dynamic range associated with individual specular (point-like) returns is important in order to discern small relative changes between two distinct target intensities when the background target field has a large intensity variation. Basically, we desire to see individual target returns from the output noise level up to some maximum level with negligible artifacts being introduced by the nonlinear action of the system prior to data processing (i.e., two-dimensional compression).

3.4 Image Contrast Ratio

The purpose of the image contrast ratio requirement is to ensure good image quality in those regions containing variations in diffuse ground returns. Such regions, for example, consist of ground painting (field patterns), roads, runways, and shadows. A low contrast image has a "washed out" appearance as though a uniform gray level or bias had been superimposed on an image which originally had considerable intensity variations from non-specular regions. To achieve a maximum image contrast ratio, reasonable control of signal independent of noise (e.g., receiver noise) and signal dependent noise (e.g., integrated sidelobe energy and radar ambiguities) must be attained.

3.5 Image Position Accuracy

The image position accuracy requirement ensures us that the resulting radar images will be adequately centered on pre-designated areas. This requirement is especially important when there is a need to image an extensive target area which completely fills the system field of view.

4.0 MEASUREMENT OF FTB IMAGE QUALITY PARAMETERS

Let us now review practical test site elements and develop a testing methodology. A practical test methodology is given for the image quality parameters outlined in Section 3.0. The tests are composed of imaging point target returns and extended targets and analyzing the resultant imagery at the output of the FTB processor. Recommended target sizes and types are given along with a general test site scenario.

4.1 Measurement of IPR Width

The 3dB IPR width can be derived from range and cross-range (azimuth) image scans of an isolated point reflector which is at least 20dB above the surrounding mean square clutter plus noise level in the image plane of the processor. Assuming manual data reduction, the output data from the FTB, corresponsing to the point target image, is passed through a two-dimensional filter which will approximate an ideal display transfer function. From Appendix C, the transfer function chosen to emulate the ideal display is a two-dimensional Gaussian filter with a spot size of 60%. This filtering action can either be accomplished by hand (with the aid of a calculator) or a computer program. From the two-dimensional Gaussian filtered data the 3dB IPR width can be measured.

Test Target

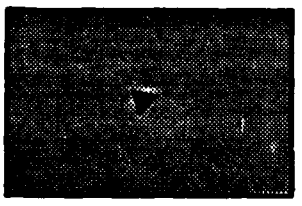

Cross-Sectional Output

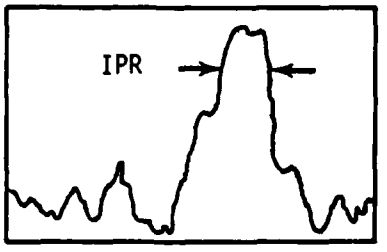

4.2 Measurement of Peak Sidelobe Level

The system sidelobe level requirement can be measured using a reflector which is at least 30dB above the mean square clutter plus noise level in the image plane of the processor.* As outlined in Section 4.1., the imagery from the output of the FTB processor is filtered with a two-dimensional Gaussian filter. From the Gaussian filtered imagery the peak sidelobe level (PSL) can be measured.

Test Target

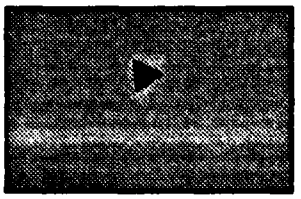

Cross-Sectional Output

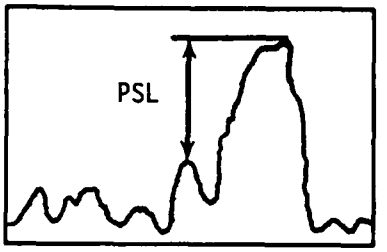

4.3 Measurement of Dynamic Range Requirements

When the above measurements are being made, it is essential for the radar system to be operating linearly. Extremely large specular reflectors or improper receiver gain settings can result in nonlinear operation which can have a profound effect on the sidelobe level and contrast ratio. The linear dynamic range (LDR) test consists of measuring the intensities of point target reflectors with known σ values. The point target reflectors should start with σ values about 10dB above the total system noise and range upward to encompass the entire linear dynamic range of the system. The measured output intensities associated with individual point returns are then plotted on a log-log scale against the known (true) σ values. The resulting data should have a linear fit to within $\pm$ 3dB up to the maximum FTB dynamic range (32dB) level above the total system noise level.

---

*The clutter plus noise power should be at least 15dB below the impulse response sidelobes being measured.

To complete the linear dynamic range measurement, it is necessary to establish the total system noise level while the radar operates linearly. Such a measurement can usually be made from a no-return area, such as a smooth lake or an extensive shadow situated near the test array of point targets. If the no-return area is not located in close proximity to the dynamic range test array, calibration must be maintained between the two test regions. This can be done, for example, by using point reflectors in each region which have an accurate (i.e., $\pm$ 1dB) relative calibration. Both test areas should have roughly the same η values to ensure that the radar is operating with nearly the same signal level at its input. Ideally, the no-return area should be situated near the largest point target for which linear operation prevails.

The size of the no-return area, ignoring edge effects, should be at least 7 resolution elements on a side if a good estimate (<1dB) of the mean square noise intensity is to be obtained from an image of the central region corresponding to 5 resolution elements on a side. This noise level estimate drops to about $\pm$1.5dB if the no-return area is only 5 resolution elements on a side with the 9 central elements available for the measurement. When the no-return area is no more than 3 resolution elements on a side, the resulting noise measurement can have an untollerably large error associated with it.

Test Targets

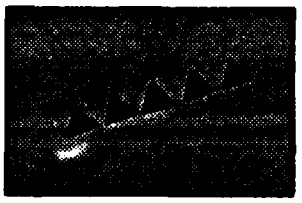

Cross-Sectional Output

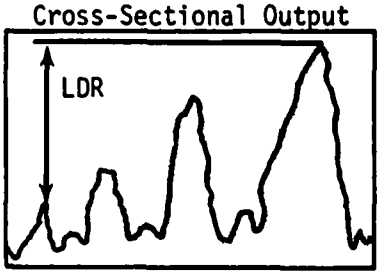

4.4 Image Contrast Ratio Measurement

To measure the image contrast ratio, the test site must have an area of extended ground clutter with known or measurable values of backscatter coefficient η such that $\sigma_0 = \eta \sin \Psi$. The principal reason for a large image contrast ratio is so that small changes in the backscatter coefficient can be perceived in the output, for example, roads, runways, and shadows which may only be a few resolution elements wide.

One way to measure the image contrast ratio is to image an extended area of relatively uniform ground clutter, which contains a small no-return area, as shown in Fig. 4-1. In this figure, region R_1 represents an area of extended ground clutter having a radar cross section density of η. The dimensions D_1 and D_2 of R_1 should be at least as large as the uncompressed range interval and the cross range illumination associated with the main lobe. Ideally, the region R_0 surrounding R_1 should have the same η value or one close to it so that the FTB processor does not experience appreciable gain variations during the course of the image contrast ratio measurement.

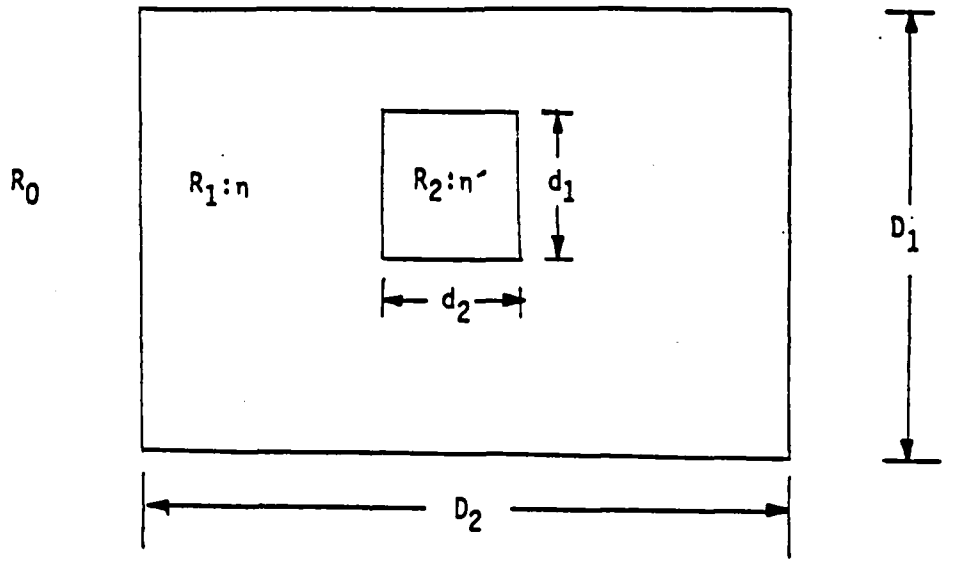

Figure 4-1. Test Site for Measuring Image Contrast Ratio.

Region R_2 should be a small no-return area. However, it will usually have a nonzero value for the backscatter coefficient η' associated with it. The dimensions d_1 and d_2 of R_2 should be large with respect to the system resolution but small relative to the instantaneous area being illuminated. These requirements on R_2 results from two needs. One is for the area of R_2 to contain many resolution elements in order to get a stable estimate of the mean value of η'. The other is the desire to have the measurement strongly influenced by the larger near-in side lobes associated with the system impulse response.

A reasonable measurement of image contrast ratio is to ratio the average image intensity associated with region R_1 by that of region R_2. When these measurements are taken one should not include the area which is within one resolution element of the boundary between regions R_1 and R_2. This area is where the primary transition from η to η' occurs in the image. Let us reflect on how the measurement accuracies of η and η' depend on the size of the respective areas over which they are measured.

We make the assumption that terrain reflectivity and the total system noise can be represented by Gaussian processes. Then to determine the average image intensities for regions R_1 and R_2, we average these two image intensities over N_1 and N_2 resolution cells, respectively. For example, if one averages the intensity of region R_2 over N_2 resolution cells to obtain an estimate of η', the RMS intensity fluctuation is nearly equal to

$$\Delta\eta' = \eta'/\sqrt{N_2}$$

for the assumed Gaussian process. That is, the measured value of η' tends to have an RMS error which is inversely proportional to the square root of the number of cells over which the measurement is made. This result is depicted graphically in Fig. 4-2. As indicated in this figure, one must average the image intensity of R_2 over at least 81 resolution cells if the RMS error in η' is to be no more than $\pm$0.5dB. Therefore, given the measurement accuracy required the size of the extended area can be found.

Test Range

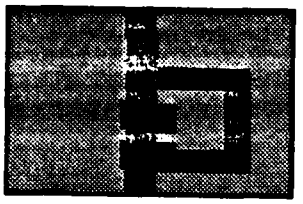

Cross-Sectional Output

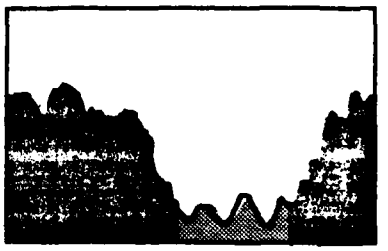

4.5 Image Position Accuracy Measurement

The reflector used to measure the IPR width can be used to determine image position accuracy if its longitude and latitude are known to have a circular error probability of less than 100 feet. From the recorded imagery the position of the reflector can be estimated and the radial position inaccuracy computed.

Test Range

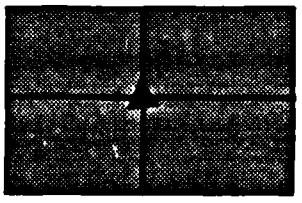

Test Range Imagery

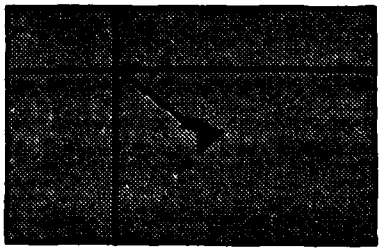

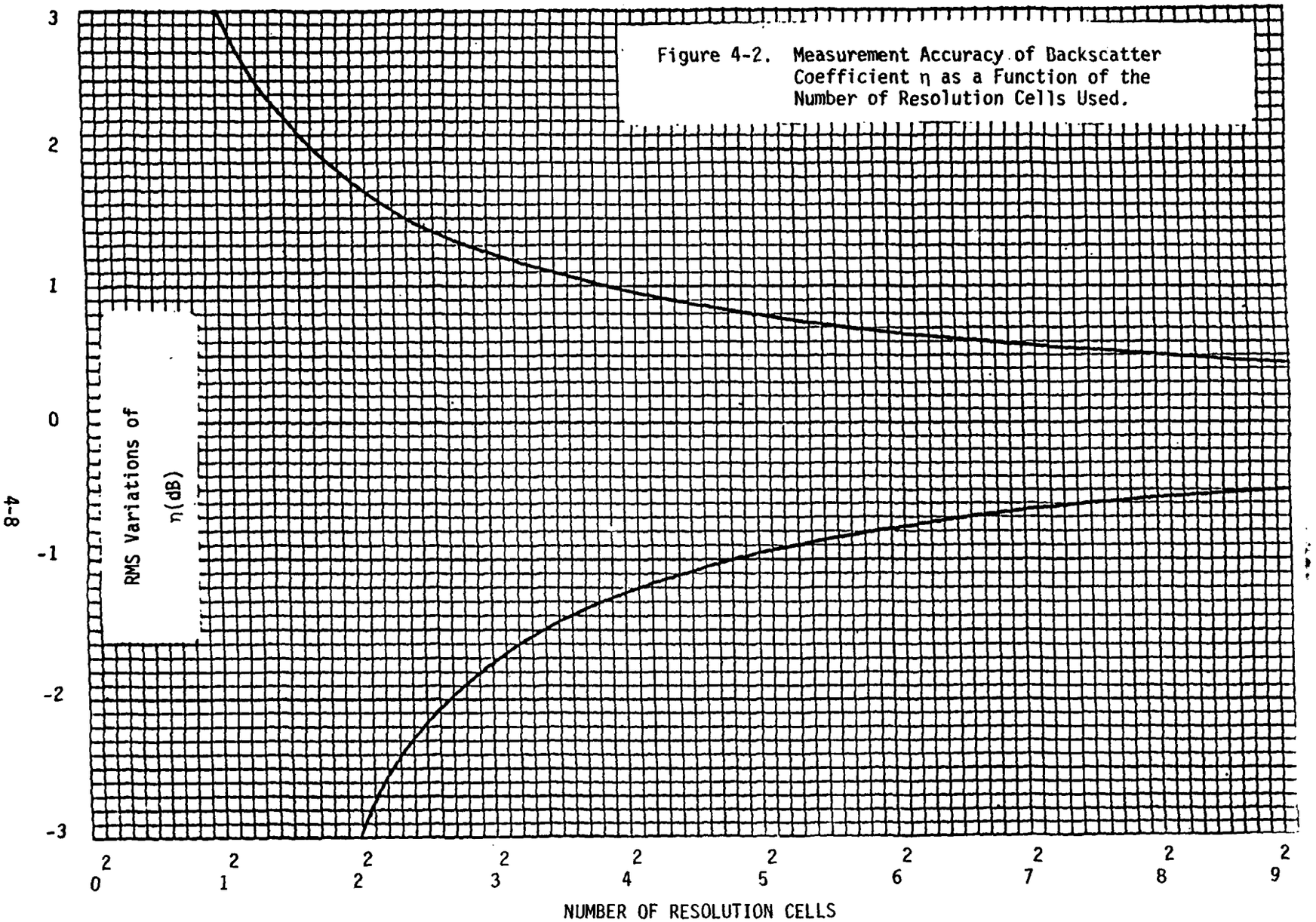

Figure 4-2. Measurement Accuracy of Backscatter Coefficient η as a Function of the Number of Resolution Cells Used.

5.0 TEST SITE CONSIDERATIONS

When considering the type and size of the reflectors to be used in the test site certain requirements must be satisfied. If the FTB processor is to be tested over a variety of operating modes (i.e., variations in ground range and/or altitude) the reflectors must provide adequate angular coverage. In Section 5.1 the angular coverage requirements to test the FTB processor are given. For dynamic range testing a bound on the maximum σ (σ_{max}) for a point target must be satisfied. By using a point target which has a cross-sectional area equivalent to σ_{max} the full dynamic range of the processor can be tested. The analysis and computation of σ_{max} is done in Section 5.2.

In Section 5.3, a list of the recommended test targets to be used is developed and presented in Table 5-1. Similarly, in Section 5.4 the extended target range is outlined.

5.1 Reflector Angular Coverage Requirements

Let us now consider the angular coverage that the test point targets must provide if the FTB is to be tested with one test site location for all ranges of operation. The grazing angle associated with an ideal spherical earth as a function of ground range for the FTB is plotted in Figs. 5-1 through 5-3. The altitudes assumed were 15,000 ft., 25,000 ft., and 35,000 ft., respectively. Note that the total angular coverage from 2.5 N.Mi. to 30 N.Mi. is about 62 deg. If the minimum testing ground range is increased to 10 N.Mi., the angular coverage that the point reflectors must provide is under 25 deg. Of the ten radar reflectors listed in Table 2, all, except the flat plate and square trihedral corner, appear to meet the above angular coverage requirements.

5.2 Maximum Point Target Requirements

Let us now consider the maximum σ values that are required to test for the linear dynamic range of the FTB. If a contrast ratio (C.R) of 3dB

Figure 5-1.GRAZING ANGLE VS. GROUND RANGE

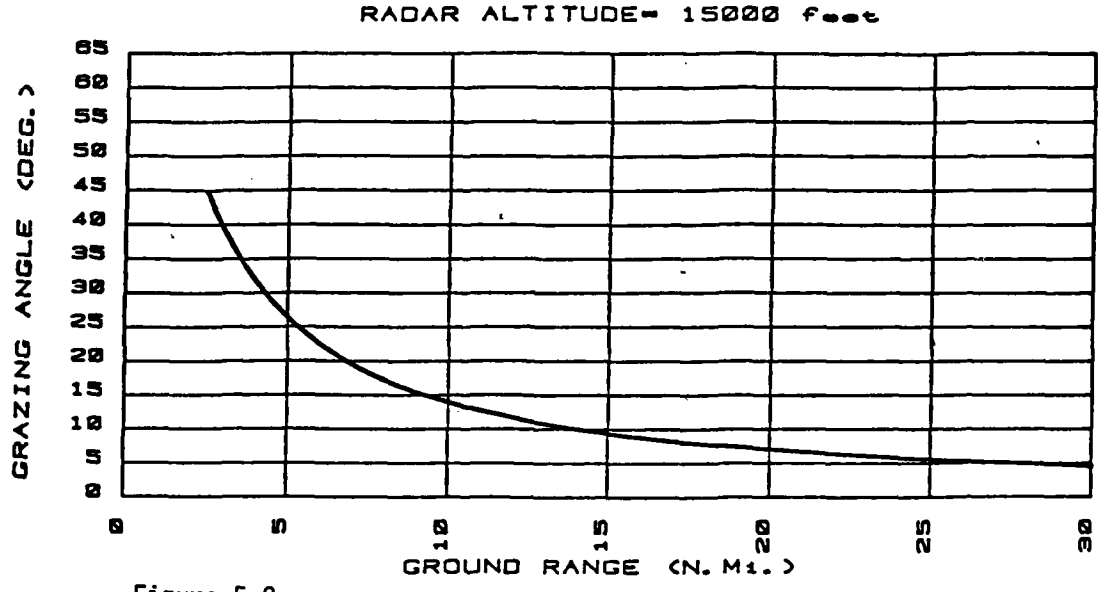

Figure 5-2.

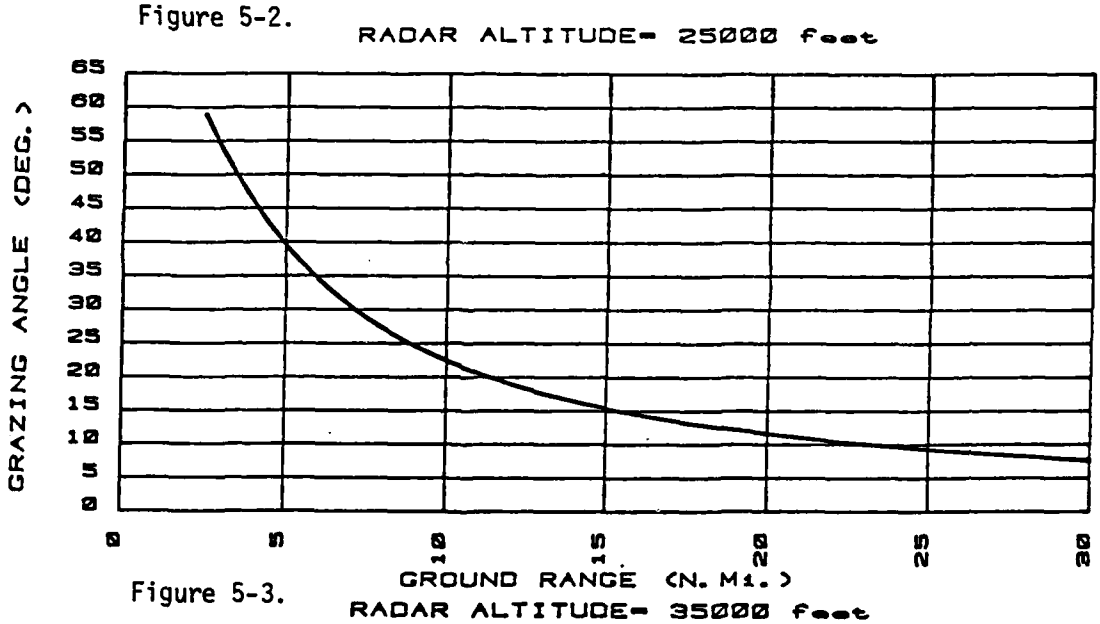

Figure 5-3.

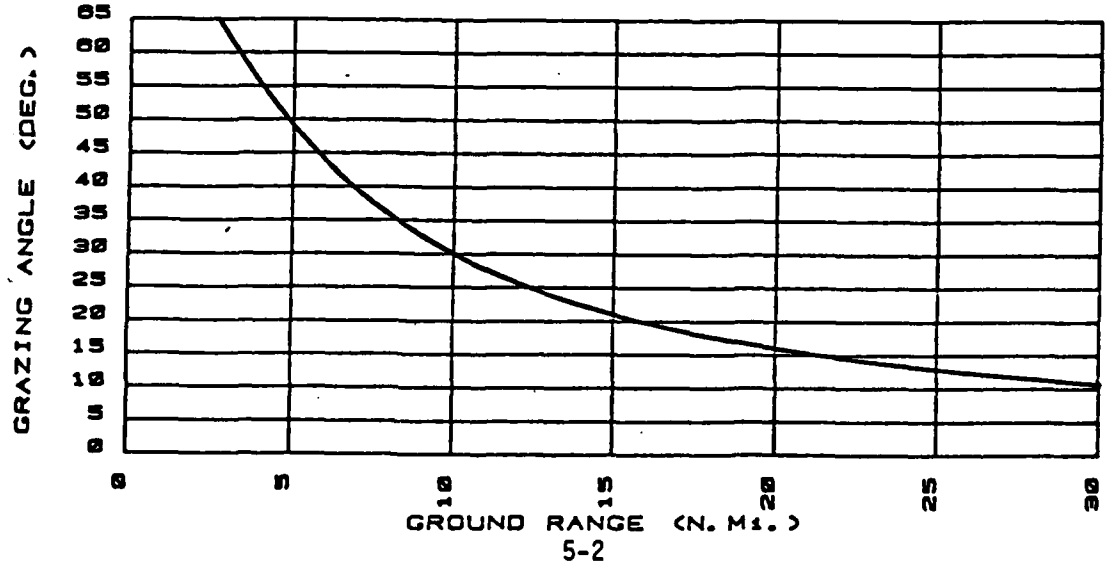

is required for a minimum η (η_m) one has to a good approximation for η_m that

$$C.R. = \frac{C_m}{N} + 1 = 2 \tag{1}$$

where C_m is clutter power corresponding to η_m and N denotes the total system noise for small input signal levels when the signal dependence noise tends to be negligibly small.

The system dynamic range is given by

$$D.R. = \frac{S_M}{N_T} \tag{2}$$

where S_M is the maximum output signal level for which linear operation is still maintained and N_T is the total noise level for large input signal levels when the signal dependent noise tends to be appreciable. Assuming that N_T and N are of the same order of magnitude in the above expressions, we can eliminate N_T from Eq. (2) to obtain

$$D.R. = \frac{S_M}{C_m} \quad . \tag{3}$$

But one typically has that

$$S_M = k\,\sigma_M \tag{4}$$

and

$$C_m = k\eta_m\rho_R\rho_c\,\tan\Psi \quad . \tag{5}$$

Here k is a constant of proportionality, ρ_R and ρ_c are the slant range and cross range resolutions, σ_M corresponds to the maximum radar cross section for which linear operation is still achieved, and Ψ is the grazing angle of the incident radiation.

Substituting Eqs. (4) and (5) into Eq. (3) and solving for σ_M yields the desired expression

$$\sigma_M = \eta_m(D.R.)\rho_R\rho_c\tan\Psi \ . \qquad (6)$$

This expression for σ_M is a low side estimate since we have not accounted for any appreciable signal dependent noise.

The FTB requirements for the 5 N.Mi. swath width mode are,

$$\rho_R = \rho_c = 20 \text{ ft.}$$

$$D.R. = 32dB = 1582$$

$$\eta_m = -10dB = 0.1 \quad \text{(assumed)}$$

Applying the above radar parameters to Eq. (6) and using the maximum required Ψ of 27 deg. which corresponds to a minimum ground range of 10 N.Mi. yields,

$\sigma_M = 32{,}242 \text{ ft}^2.$
For 5 N.Mi. swath width mode

5.3 Recommended Point Targets

Let us now consider what size passive reflectors are required to conduct a FTB dynamic range test. From the above analysis we determined that σ_M should be at least $3.2 \times 10^4 \text{ft.}^2$. Actually it should be about 5dB larger, $10 \times 10^4 \text{ft.}^2$, in order to account for the angular dependence of σ and for some signal dependent noise. From a detection theory point of view, the minimum size reflector should be about 5dB above the total system noise level. Since the total system noise, N_T, is approximately 29ft.^2 the minimum size reflector should be about 100ft.^2. To get a reasonable amount of data for establishing the linear dynamic range of the FTB, successive σ values should increase by approximately a factor of 5dB.

The physical sizes of candidate reflectors for testing the FTB dynamic range are given in Table 5-1. In the construction of this table a nominal wavelength of 0.1 ft. has been assumed. The minimum reflector dimensions are required to be at least 3λ. The maximum practical reflector dimensions are limited to 6.5 ft.

From Table 2-1, Appendix B and Figs. 5-1 through 5-3, triangular trihedral corner reflectors can provide adequate angular coverage for all ground ranges of interest. Table 5-1 indicates that these reflectors can have σ values ranging from 100 $ft.^2$ to $10^5 ft.^2$. The corresponding reflector edge dimensions range from .7 ft. to 3.9 ft. The square-trihedral corner reflector edge dimensions are approximately 40% less than the corresponding triangular trihedral reflector. However, according to Table 2, the trihedral corner reflectors do not provide as much angular coverage as the triangular ones.

The Luneberg lens was not included in Table 5-1. However, they are often used as calibration standards of σ since they can provide a large angular coverage with rapid cutoff between their broad main lobe and their side lobes. A typical normalized radar cross section versus grazing angle plot for a Luneberg lens is presented in Fig. 5-4. Note that the radar cross section decreases over 20dB from the 3dB point as the incidence angle is increased an additional 3 deg. Luneberg lenses can provide economical radar cross sections ranging from about $10 ft.^2$ up to 3200 $ft.^2$. Typical 1,000 $ft.^2$ calibration references are a little over one foot in diameter.

Since the popular triangular trihedral corner reflector can be used for much of the FTB processor image quality testing, let us review the angular coverage which they theoretically can provide. Using the

TABLE 5-1

PHYSICAL SIZES OF DYNAMIC RANGE REFLECTORS FOR λ = 0.1 ft.

σ(ft.^{2})	DECIBEL LEVEL (100 ft^2=0dB)	EDGE OF A TRIANGULAR TRIHEDRAL CORNER (ft.)	EDGE OF A SQUARE TRIHEDRAL CORNER (ft.)	LENGTH BY WIDTH (EDGE) OF A DIHEDRAL CORNER SURFACE (ft. x ft.)
100	0dB	0.699	0.404	0.447 x 0.447
320	5dB	0.935	0.540	0.597 x 0.597
10^3	10dB	1.24	0.718	0.794 x 0.794
3.2×10^3	15dB	1.66	0.960	1.06 x 1.06
10^4	20dB	2.21	1.28	1.41 x 1.41
3.2×10^4	25dB	2.96	1.71	1.89 x 1.89
10^5	30dB	3.93	2.27	2.51 x 2.51

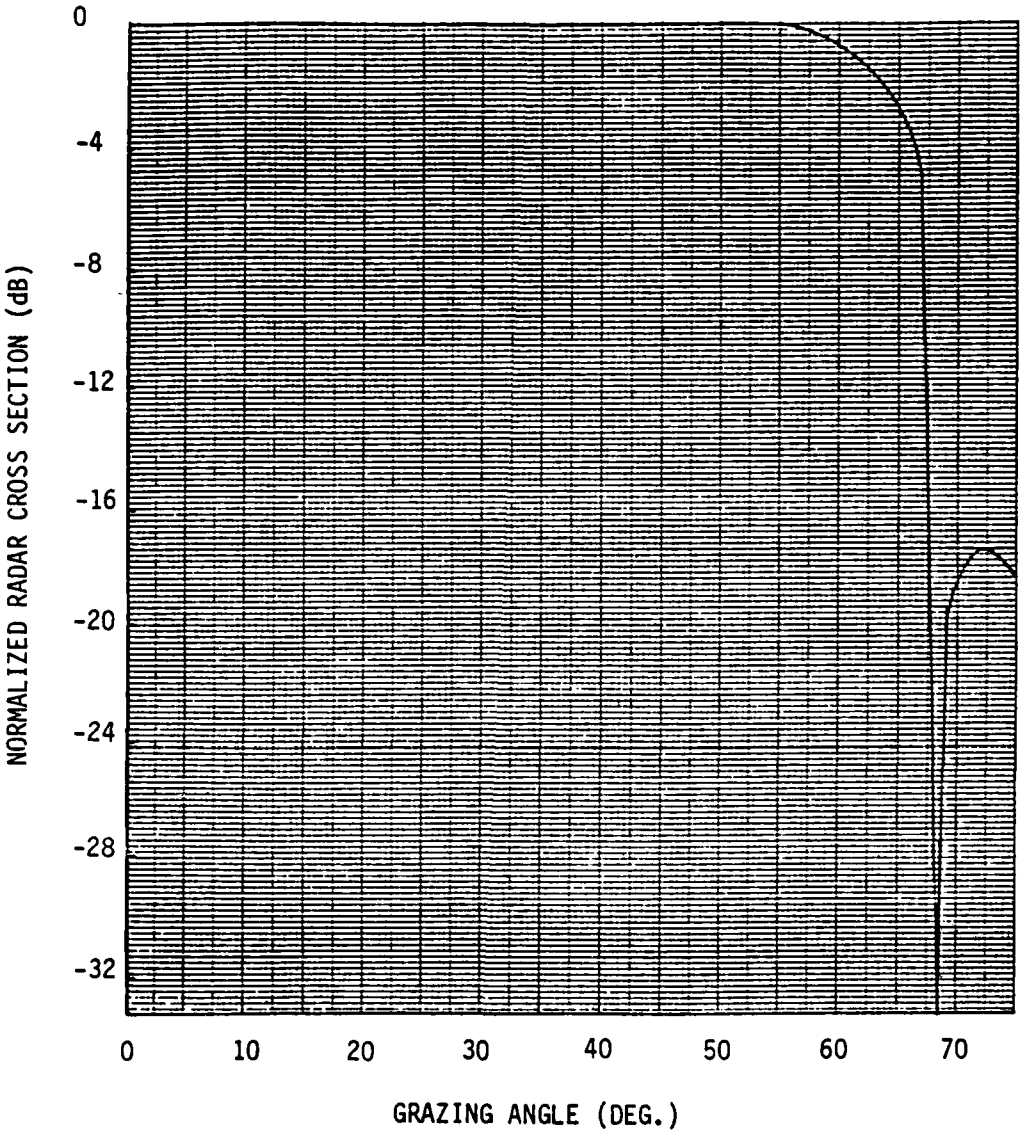

Figure 5-4. Normalized Radar Cross Section vs Grazing Angle for a Luneberg Lens.

equation given in entry 5 of Table A-1, we can plot the normalized radar cross section as a function of grazing angle as shown in Fig.5-4. Note that the elevation pattern has a 3dB elevation width of about 40 deg. centered at a grazing angle of 35.3 deg. Reviewing Figs. 5-1 through 5-3, we we observe that the FTB processor only requires an elevation coverage of 25 deg. (if we assume the minimum ground range for testing purposes is 10 N.Mi.). In order to obtain adequate elevation coverage at the lower grazing angles ($\Psi < 16^{o}$), the triangular trihedral corner reflector should be tilted downward approximately 20 degrees.

When corner reflectors are tilted downward, serious ground interference problems can result between the direct radar return and one which returns via a ground reflection. One way to reduce ground interference problems is to place some microwave absorbing material in the region where most of the ground reflection is occuring. For the larger corner reflectors this solution is not very practical since the required area of the absorbing material would be hundreds of square feet.

Another approach to the ground bounce problem is to elevate the reflector sufficiently high above the earth so that direct and indirect returns are at least two slant range resolution elements apart. One can show that the direct return and indirect return appear to be separated a distance

$$\Delta r = 2h\sin\Psi$$

where h is the normal distance of the reflector above the ground plane (earth), and Ψ is the grazing angle.

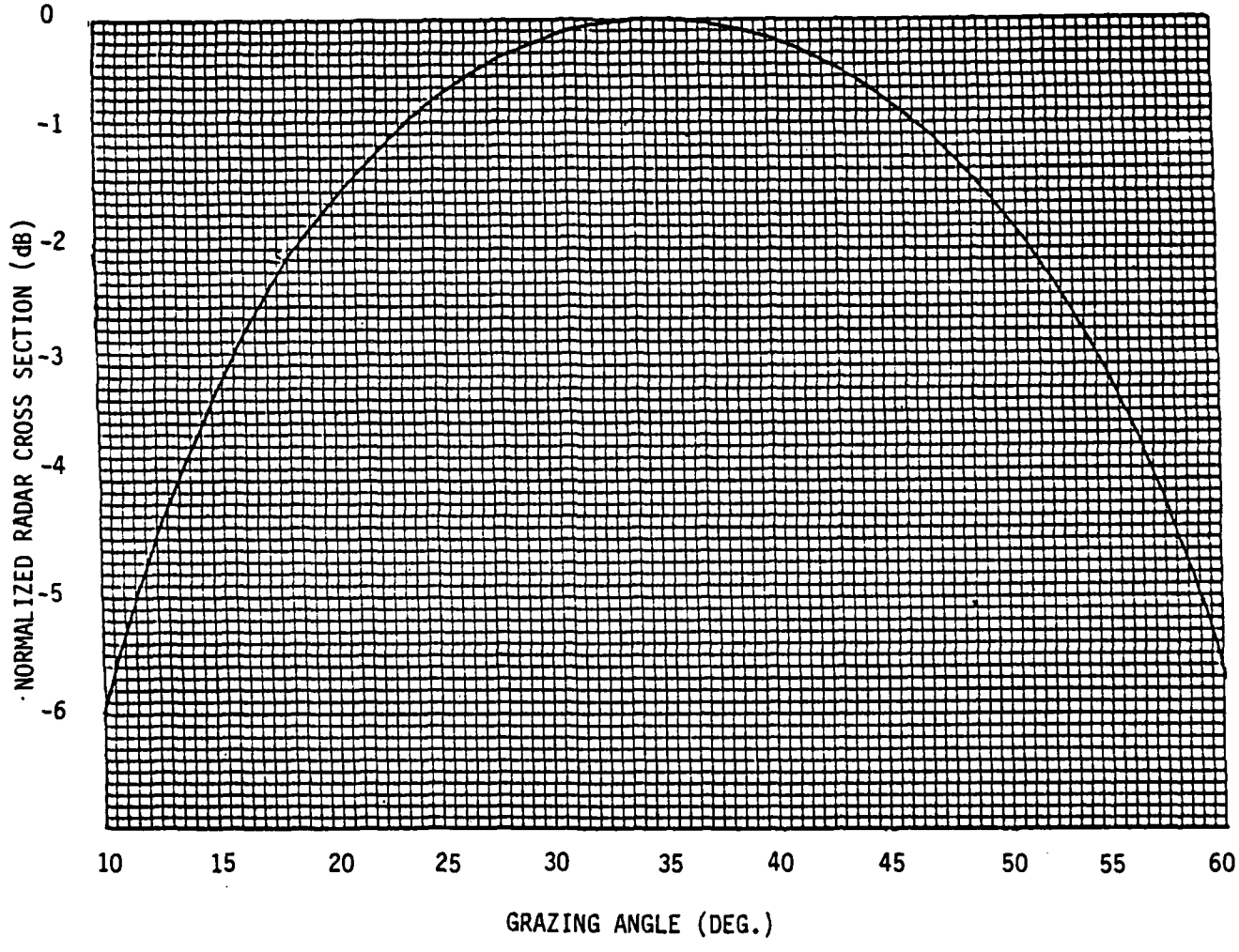

Figure 5-5. Normalized Radar Cross Section vs Grazing Angle for a Triangular Trihedral Corner Reflector.

Solving for h one obtains

$$h = \frac{\Delta r}{2 \sin \Psi}$$

Now let

Δr = 60 ft. (3 resolution elements)

Ψ = 3 deg.

The resulting value for h is

h = 573 ft.

which is a pretty high pedestal for a corner reflector. However, a high hill or the side of a mountain could be used to eilminate ground bounce by altering the ground reflection angle. To greatly suppress the specular ground bounce the trihedral corner reflector should be placed on a local terrain slope of at least 10 deg. Thus, it appears that potential ground bounce problems could be greatly alleviated by selecting a test site on the side of a foothill or mountain.

5.4 Recommended Extended Targets

Having reviewed the measurement procedures for measuring image contrast ratio in Section 4.4, we can now consider the test site requirements for extended targets. Ideally, there should be several large areas with respect to the uncompressed signal area. Each area should have a different, known average η value; and each should contain a small no-return area whose dimensions are about 10 resolutions (200 ft.) on a side. Probably at least three measurements should be made, namely, at approximate η values of -18dB, -5dB, and greater than 0dB. It should not be too difficult to find a natural terrain (e.g., grassland or desert) which has an η value around -18dB.

However, the other two η values are larger than most of those provided by mother nature. For the larger η values, man-made structures in suburban and urban areas could be used.

The small no-return area within the uniform extended terrain can be constructed, if necessary, since its required dimensions are between five and ten resolution elements on a side. Actually, the so called no-return area can have a nonzero backscatter coefficient providing it is at least 10dB smaller than the total system noise level (approximately $\eta \approx$ -30dB).

6.0 TEST SITE RECOMMENDATIONS

Previous sections of this report have discussed FTB performance requirements, measurements and the various components of a test range. This section will bring all of these elements together and recommend a general test site design for the FTB. Using this recommended design, the next step would be selecting an actual ground site and finalizing the design.

When measuring the FTB image quality parameters there are two basic types of measurements performed, namely, linear and nonlinear. If both types of measurements are made during a single flight line (pass), then the linear measurements should be made first. The reason for this is that a SAR system experiencing nonlinear effects from strong target returns may not recover in time to perform adequately during subsequent linear testing.

The placement of the reflectors within the radar test range deserve a certain amount of consideration. The major sidelobes from the reflectors occur approximately every 1 to 2 resolution elements apart and lie parallel and perpendicular to the flight path. By placing the reflectors in a line diagonal to the flight path, the contamination of one image with another image's sidelobe energy is minimized. The interference of one image's sidelobes with another's mainlobe should be kept below -15dB of the mainlobe. Assuming the adjoining reflectors vary in size by 10dB the spacing should be adequate to keep the sidelobe interference below -25dB. If the reflectors are placed diagonal to the flight path a spacing distance of 5 resolution elements will be adequate to keep the sidelobe interference below -30dB.

The recommended linear and nonlinear test ranges are illustrated in Figs. 6-1 and 6-2. Listed in Table 6-1 are the image quality parameters to be measured with each reflector illustrated in Figs. 6-1 and 6-2. The linear test range, Fig. 6-1, is composed of six point target reflectors with cross sectional area (σ) ranging from 100 ft^2 to 10,000 ft^2. Note that #C1 is a calibrated reference target, and therefore it should be a high quality Luneberg lens reflector. By placing reflector #C1 at a known latitude and longitude, it can also be used for the image position accuracy measurement. The aircraft flight path should be oriented such that the flight directional angle, γ, is $90^0 \pm 5^0$ in order to keep the cross sectional area inaccuracies to within $\pm$ 0.5dB and so that no significant sidelobe energy associated with the image of one contaminates the image of another.

TABLE 6-1. IMAGE QUALITY PARAMETER MEASURED AS A FUNCTION OF TEST RANGE TARGET

Point Target (Reflector)	Cross-Sectional Area ∿ (σ) (ft^2)	IMAGE QUALITY MEASUREMENTS				
		IPR Width	Peak Sidelobe Level	Linear Dynamic Range	Image Position Accuracy	
#1	100			✓		
#2	320			✓		Notes
#3	1,000	X	X	✓		✓ - Recommended
#4	3,200	X	X	✓		X - Possible
#5	10,000	✓	✓	✓	X	
#6	32,000			✓		
#7	100,000			✓		
#C1	$320 \leq \sigma_0 \leq 3,200$			✓	✓	
#C2	$320 \leq \sigma_0 \leq 3,200$			✓	X	

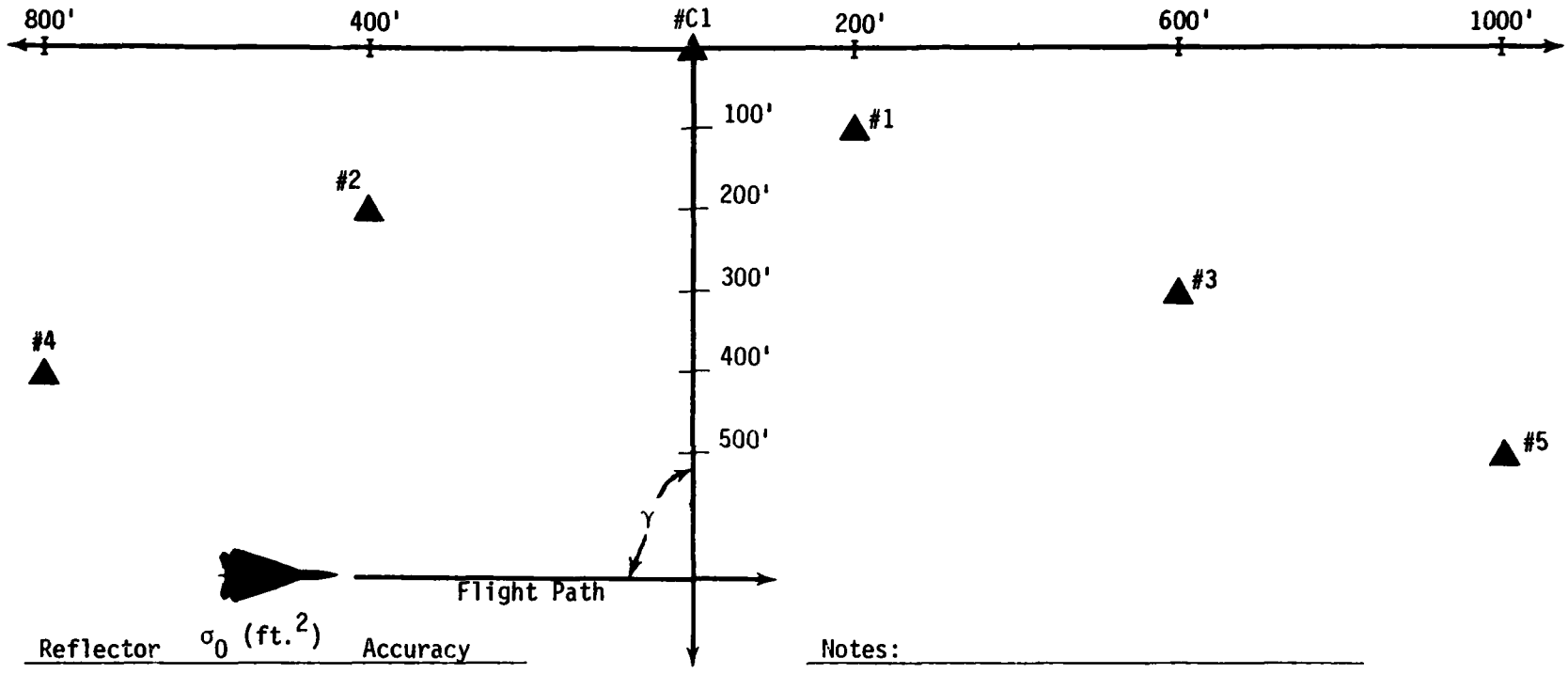

Reflector	σ_0 (ft.^{2})	Accuracy
#1	100	≤ 1dB
#2	320	≤ 1dB
#3	1,000	≤ 1dB
#4	3,200	≤ 1dB
#5	10,000	≤ 2dB
#C1	> 320 and ≤ 3,200	≤ .5dB

Notes:

1. All dimensions are in feet
2. All distances are measured from #C1
3. All reflectors are tilted downward $8^0 \pm 2^0$
4. Reflector placement accuracy should be within ± 25 ft., referenced to #C1.

Figure 6-1. Recommended Linear Test Range.

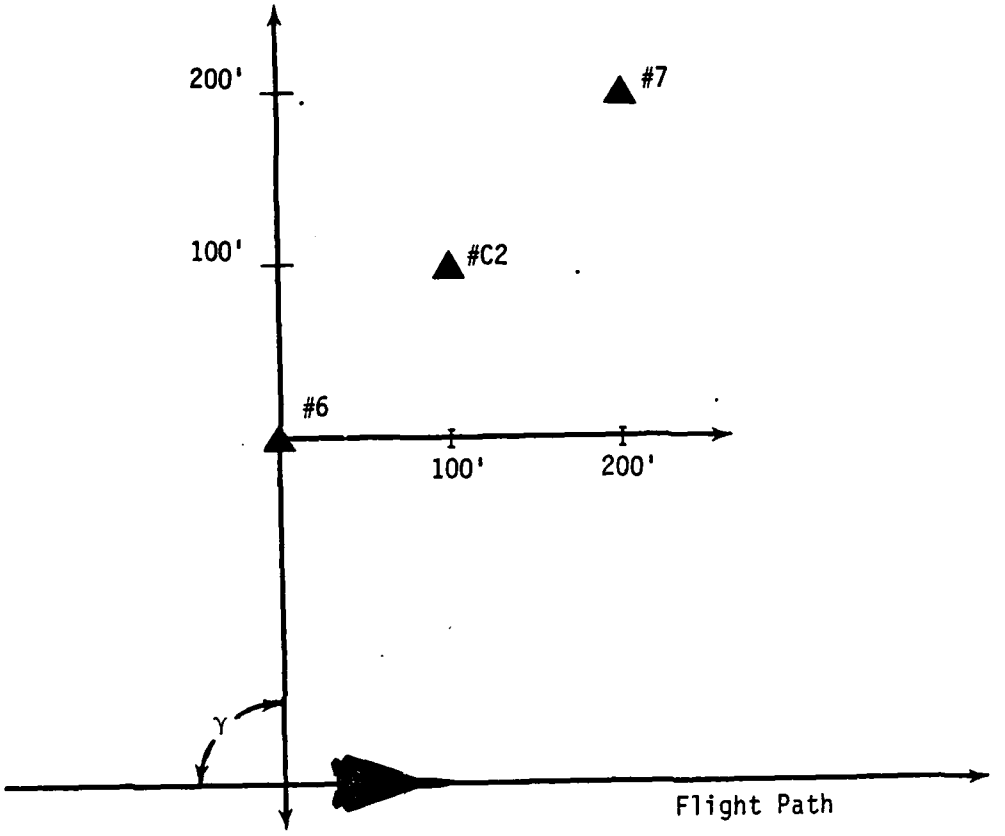

Reflector	$\sigma_0(ft.^2)$	Accuracy
#6	3.2×10^4	$\leq$ 2dB
#7	1.0×10^5	$\leq$ 2dB
#C2	$\begin{cases} > 320 \\ < 3,200 \end{cases}$	$\leq$ 1dB

Notes:

1. All dimensions are in feet
2. All distances are measured from reflector #6
3. All reflectors are tilted downward $8^0 \pm 2^0$
4. Reflector placement should be within $\pm$25 ft., referenced to #6.

Figure 6-2. Proposed Non-Linear Test Range.

The nonlinear test range, Fig. 6-2, is composed of three point target reflectors, a calibrated reference target and two large reflectors. As with the linear test range, the calibrated reference source should be a Luneberg lens reflector and the same requirements on γ apply. The placement of the nonlinear range should be such that the radar should only be experiencing the effects of one of the ranges (linear or nonlinear) for a period of time at least as long as the coherent integration time (i.e., the time to fly a synthetic aperture). Two proposed orientations of the radar ranges are illustrated in Fig. 6-3.

The required reflector angular and cross sectional coverage can be realized with all the reflectors mentioned in section 2, except flat plates.

Using any of the reflectors the radar range can be used for grazing angles (γ) from 10 degrees to 40 degrees before experiencing a loss in cross sectional area (σ_0) greater than 3dB. Using the above restriction, the allowable operating flight paths for the radar platform are illustrated in Fig. 6-4.

Let us now consider the extended target requirement. As stated in section 4 the image contrast ratio measurement requires the use of extensive terrain containing at least one small no-return area. The no-return area should ideally be about 10 resolution elements (200 feet) on a side (e.g., airfield, river, pond). The η values associated with the return area should be approximately -18dB.

A number of calibrated point targets should be placed in each area of extended terrain that is used for image contrast ratio measurements.

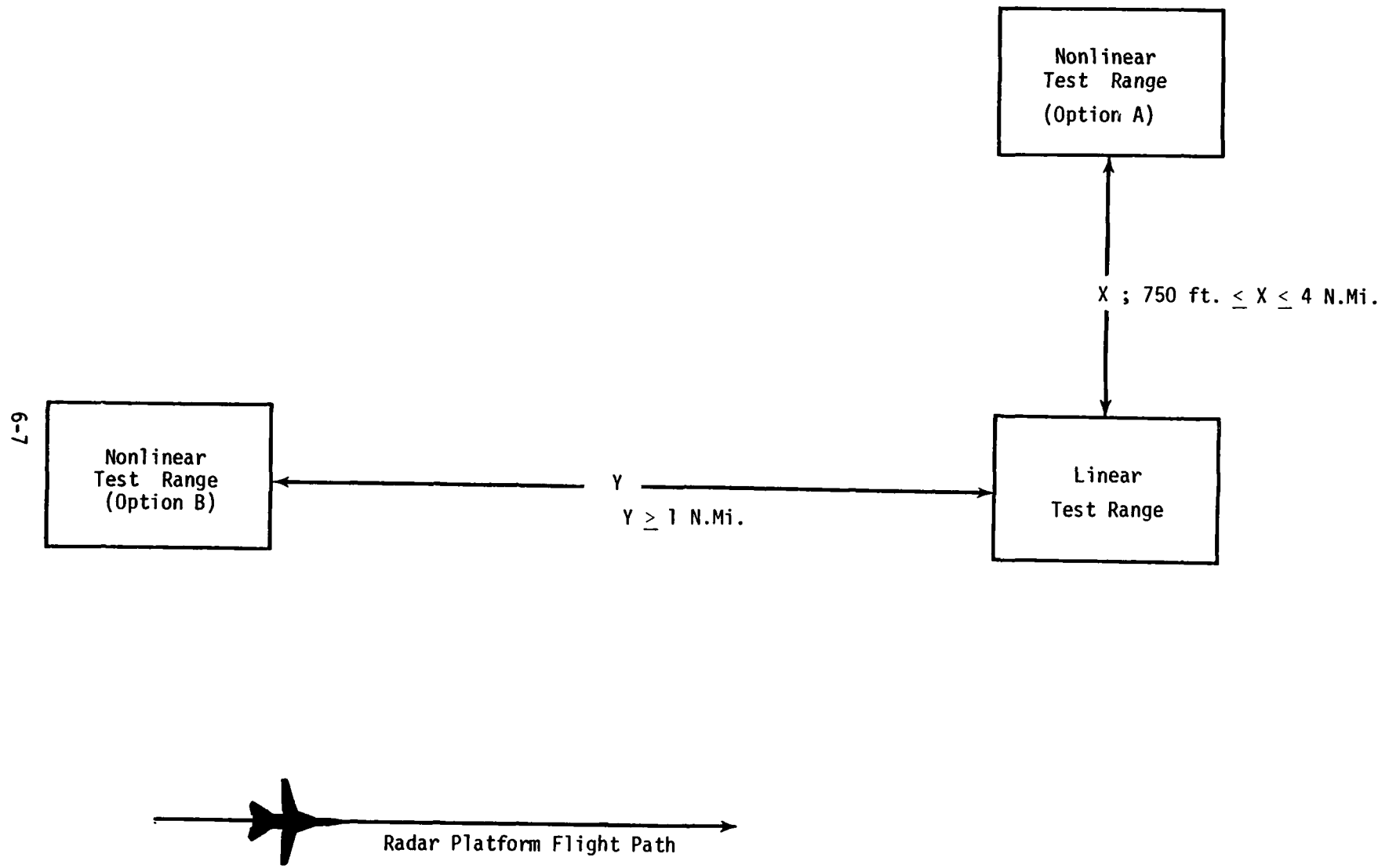

Figure 6-3. Orientation and Placement of Linear and Non-Linear Test Ranges.

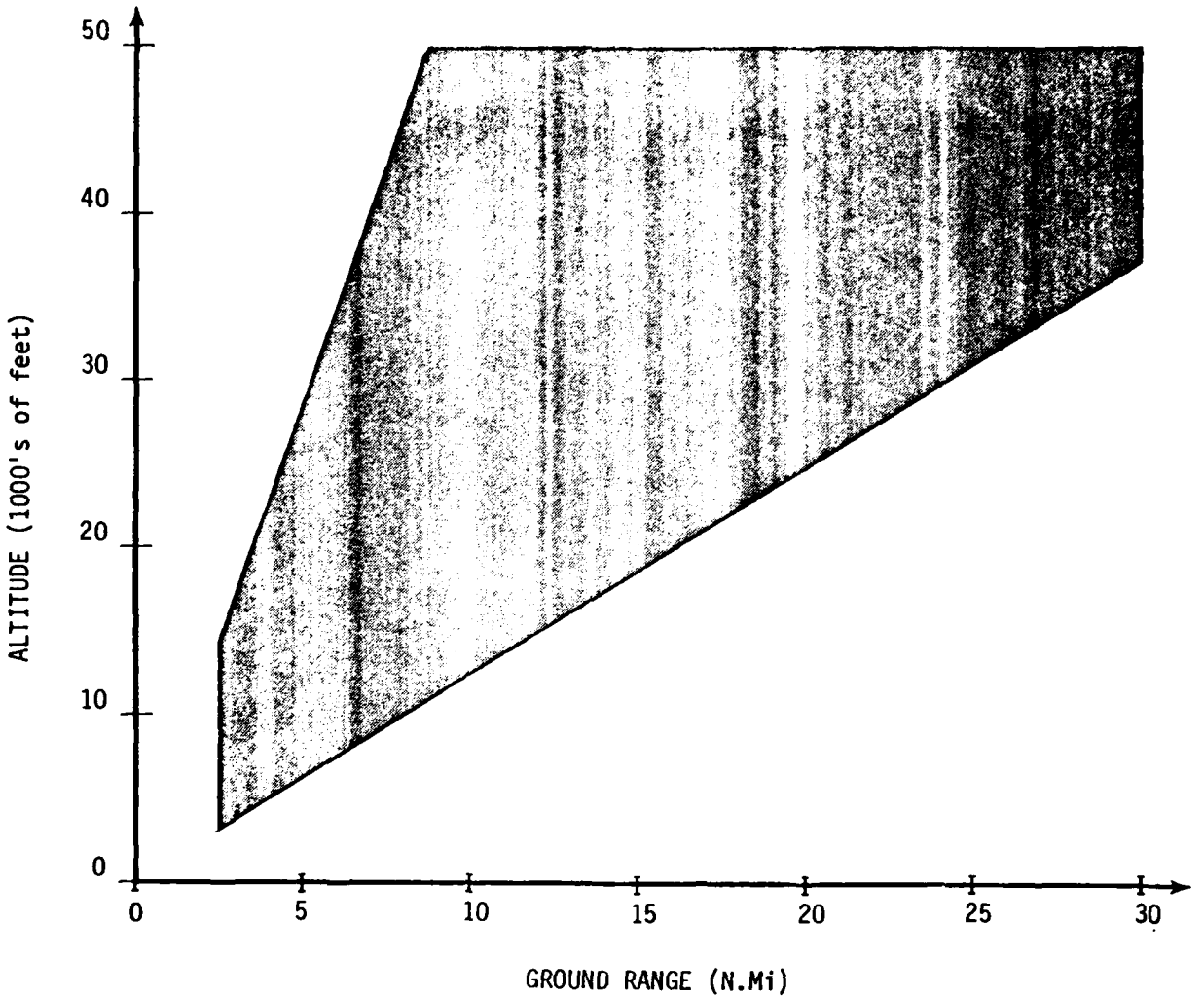

Figure 6-4. Platform Operating Limits for the Recommended FTB Test Range.

Then the actual η values associated with each terrain type can be accurately estimated by making relative image intensity measurements between patches of terrain and the individual reference targets. To improve the accuracy of the η estimates, one could use several reference targets and average their resulting intensities.

BIBLIOGRAPHY

1. Sofianos, D. J., "Optimum Gaussian-Shaped Writing Beams for Compressed Radar Imagery," An Internal Report, May 22, 1979.

2. Cotter, C., "Optimization of a Laser Beam Recorder for the Display of Compressed Radar Images," An Internal Report, October 12, 1979

3. Sofianos, D. J., "Interpolation of Point Target Returns," An Internal Report, July 5, 1979.

4. Cotter, C., "An Initial Study of PTS Bandwidth Reduction by Data Up-Sampling," An Internal Report, December 14, 1979.

5. Zelenka, J. S. and D. J. Sofianos, "Initial Findings on the Displaying of Digitally Processed SAR Data," An Internal Report, September 18, 1978.

6. Sofianos, D. J., T. Falk, and D. A. Phillips, "Initial Results on Gaussian Interpolation of Digital SAR Data," An Internal Report, November 13, 1978.

APPENDIX A

BEAM PATTERNS OF SPECULAR REFLECTORS

by
Jerry Zelenka

Let us now review the backscatter radar cross section for a number of the ideal reflectors presented in Section 2. We assume that the reflector dimensions are large with respect to the wavelength (i.e., dimensions $\geq 3\lambda$), that all reflector surfaces are perfectly smooth and 100% reflective, and that all corners are perfectly square. In addition, all backscatter from edge effects are ignored so that we can utilize the relatively simple physical-optics techniques. For the above assumptions, we have the results presented in Table A-1. In this table, (x,y,z) denote the coordinates of a right-handed coordinate system. The corresponding sperical coordinates are denoted by (R,θ,ϕ). The sinc $(\cdot)$ function which appears many times in Table A-1 is defined as

$$\text{sinc } x = \frac{\sin \pi x}{\pi x} \tag{A-1}$$

TABLE A-1

REFLECTOR RADAR CROSS SECTIONS DEPENDENCE ON LOOK ANGLE

Reflector Description	Radar Cross Section As A Function Of The Radar Angular Location
1. Rectangular Flat Plate having its center at the origin and its normal parallel to the z-axis. It has a width W in x and a length L in y.	$\sigma = \frac{4\pi W^2 L^2}{\lambda^2} (\cos\theta)^2 \times \left[\text{sinc}\left(\frac{W}{\lambda}\sin\theta\cos\phi\right)\right]^2 \times \left[\text{sinc}\left(\frac{L}{\lambda}\sin\theta\sin\phi\right)\right]^2$ for $0 < \theta < 90^0$ and for all ϕ.
2. Finite Circular Cylinder of diameter d and length L. It is centered at the origin and has its axis parallel to z.	$\sigma = \frac{\pi d L^2}{\lambda} (\sin\theta)^2 \times \left[\text{sinc}\left(\frac{L}{\lambda}\cos\theta\right)\right]^2$ for all θ and all ϕ.
3. Sphere of diameter d centered at the origin.	$\sigma = \frac{\pi}{4} d^2$ for all θ and σ.

TABLE A-1 Continued

4. Dihedral Corner consisting of two identical rectangular plates of dimensions W by L. The common edge of width W is oriented along the y-axis, and it is centered at the origin. One plate is in the x-y plane and the other is in the y-z plane.	$\sigma = \frac{8\pi W^2 L^2}{\lambda^2} \left[\text{sinc}\left(\frac{W}{\lambda}\sin\right)\right]^2 \times 1 - \sin\lvert 2\theta - 90^0\rvert$, for $0 < \theta < 90^0$ and $\lvert\phi\rvert < 90^0$.
5. Triangular Trihedral Corner with the edges of the intersecting surfaces situated along the positive x-, y-, and z-axes for a distance of L from the origin. The maximum radar cross section occurs at $\theta = \hat{\theta} = \tan^{-1}\sqrt{2}$ and $\phi = 45^0$.	$\sigma = \frac{4\pi L^2}{\lambda^2} \times \left\{\lvert\cos\theta + \sin\theta\,(\sin\phi + \cos\phi)\rvert - 2\,\lvert\cos\theta + \sin\theta\,(\sin\phi + \cos\phi)\rvert^{-1}\right\}^2$ for $\theta = \hat{\theta} \pm 20^0$ and for $\phi = 45^0 \pm 20^0$ where $\hat{\theta} = \tan^{-1}\sqrt{2} = 54.74^0$.
6. Top Hat consisting of a circular cylinder of diameter d and length L with its axis along the z-axis and its base centered on a circular base of diameter D in the x-y plane.	$\sigma = \frac{4\pi d L^2}{\lambda}\sin\theta$ for $0 < \theta < \tan^{-1}\left(\frac{D - d}{2L}\right)$ and for all ϕ.
7. Luneberg Lens of diameter d having its center at the origin and its axis along the z-direction.	$\sigma \approx \frac{\pi^3 d^4}{4\lambda^2}$ for $\theta \leq 65^0$ and for all ϕ.

APPENDIX B

ALIGNMENT REQUIREMENTS FOR CORNER REFLECTORS

by
Jerry Zelenka

The monostatic radar cross section associated with dihedral and trihedral corner reflectors is highly dependent upon the squareness or alignment of the individual surfaces. In fact, the monostatic radar cross section of corner reflectors tends to decrease very quickly as one or more surfaces becomes slightly misaligned. We now show how the radar cross section for dihedral and trihedral corner reflectors depends upon their surface misalignment. All surfaces are assumed to be perfectly flat. That is, the effects of bowing or sagging surfaces will not be considered.

We begin by reviewing the basic vector relationships between an arbitrary ray incident upon a planar surface S and the corresponding reflected ray as shown in Fig. B-1. In this Figure $\overline{N}$ is a unit vector normal to the surface S. The unit incident ray and reflected ray are denoted by $\overline{I}$ and $\overline{R}$, respectively.

Since all three vectors indicated in Fig. B-1 must be coplanar, one can write

$$\overline{I} \cdot (\overline{N} \times \overline{R}) = 0 \qquad \text{(B-1)}$$

The projection of $\overline{I}$ into the surface S must be equal to the projection of $\overline{R}$ into the surface S. Hence, one has

$$\overline{I} \times \overline{N} = \overline{R} \times \overline{N}, \qquad \text{(B-2)}$$

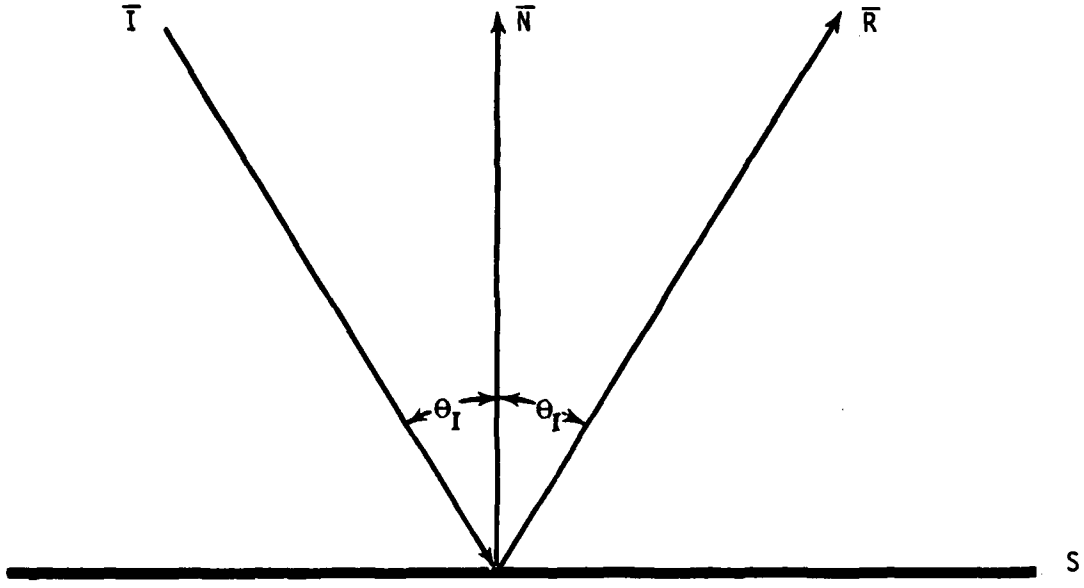

FIG. B-1. Geometry for Incident and Reflected Rays.

which can be rewritten as

$$(\overline{I} - \overline{R}) \times \overline{N} = 0 \tag{B-2'}$$

The component of $\overline{I}$ which is normal to S must be equal to the component $\overline{R}$ which is normal to S. Therefore, one has

$$- \overline{I} \cdot \overline{N} = \overline{R} \cdot \overline{N}, \tag{B-3}$$

which can be rewritten as

$$(\overline{I} + \overline{R}) \cdot \overline{N} = 0. \tag{B-3'}$$

Since $\overline{I}$ and $\overline{R}$ have been normalized to unity, we can write

$$|\overline{I}| = |\overline{R}| = |\overline{N}| = 1. \tag{B-4}$$

Let the three vectors under consideration have the following sets of direction cosines:

$$\overline{I} = (\alpha,\beta,\gamma) \tag{B-5}$$

$$\overline{N} = (a,b,c) \tag{B-6}$$

and

$$R = (\alpha',\beta',\gamma'). \tag{B-7}$$

We now show that the direction cosines, α', β', and γ', can be expressed in terms of the other direction cosines, namely, α, β, γ, a, b, and c.

According to Eq. (B-1), we can write

$$\begin{vmatrix} \alpha & \beta & \gamma \\ a & b & c \\ \alpha' & \beta' & \gamma' \end{vmatrix} = 0 \tag{B-8}$$

or

$$\alpha'(\beta c - \gamma b) + \beta'(\gamma a - \alpha c) + \gamma'(\alpha b - \beta a) = 0 \qquad \text{(B-9)}$$

From Eq. (B-2'), we have

$$\begin{vmatrix} \bar{i} & \bar{j} & \bar{k} \\ (\alpha' - \alpha) & (\beta' - \beta) & (\alpha' - \gamma) \\ a & b & c \end{vmatrix} = 0 \qquad \text{(C-10)}$$

oθ

$$0 + c\beta' - b\alpha' = \beta c - \gamma b, \qquad \text{(C-11)}$$

$$-c\alpha' + 0 + a\gamma' = \gamma a - \alpha c, \qquad \text{(C-12)}$$

$$b\alpha' - a\beta' + 0 = \alpha b - \beta a. \qquad \text{(C-13)}$$

From Eq. (B-3'), we have

$$a\alpha' + b\beta' + c\gamma' = -\alpha a - \beta b - \gamma c. \qquad \text{(B-14)}$$

Of the above five equations in α', β', and γ', we require the use of three that are independent. We choose Eqs. (B-9), (B-11), and (B-14) to solve for α', β', and γ'. The resulting expressions are then simplified by applying Eq. (B-4). We finally obtain

$$\alpha' = \alpha(1 - 2a^2) - 2a(\beta b + \alpha c), \qquad \text{(B-15)}$$

$$\beta' = \beta(1 - 2b^2) = 2b(\alpha a + \gamma c), \qquad \text{(B-16)}$$

$$\gamma' = \gamma(1 - 2c^2) = 2c(\alpha a + \beta b). \qquad \text{(B-17)}$$

Consider the ideal triangular trihedral corner reflector shown in Fig. B-2. The three surfaces lie in the x-y, x-z, and y-z planes; and they are denoted by a, b, and c, respectively. The vertex of the corner lies at the origin, and the three edges lie along the positive x-, y-, and z-axes. The leg of each triangular surface has a length L.

For the corner reflector shown in Fig. B-2, let there be an incoming ray that falls on surface a, then deflects to surface b, then deflects to surface c and finally returns back toward its original source. Actually, the surface order is not important. For this ideal corner reflector case and those considered below with misalignments all six surface combinations lead to the same result for the direction of the outgoing ray.

The incoming ray can be represented as

$$I_a = (\alpha,\beta,\gamma), \tag{B-18}$$

and the three surface normals are

$$N_a = (0,0,1), \tag{B-19}$$

$$N_b = (1,0,0), \tag{B-20}$$

and

$$N_c = (0,1,0). \tag{B-21}$$

Applying Eqs. (B-18) and (B-19) to Eqs. (B-15)-(B-17), one finds that the ray reflecting off surface a and then impinging on surface b is

$$R_a = I_b = (\alpha,\beta,-\gamma). \tag{B-22}$$

Repeating the above exercise for the second surface, one finds that the ray reflecting off of surface b and impinging on surface c is

$$R_b = I_c = (-\alpha,\beta,-\gamma). \tag{B-23}$$

When the reflection from the third surface is considered, one finds that the outgoing ray, which is reflecting off of surface c, is

$$R_c = (-\alpha,-\beta,-\gamma). \tag{B-24}$$

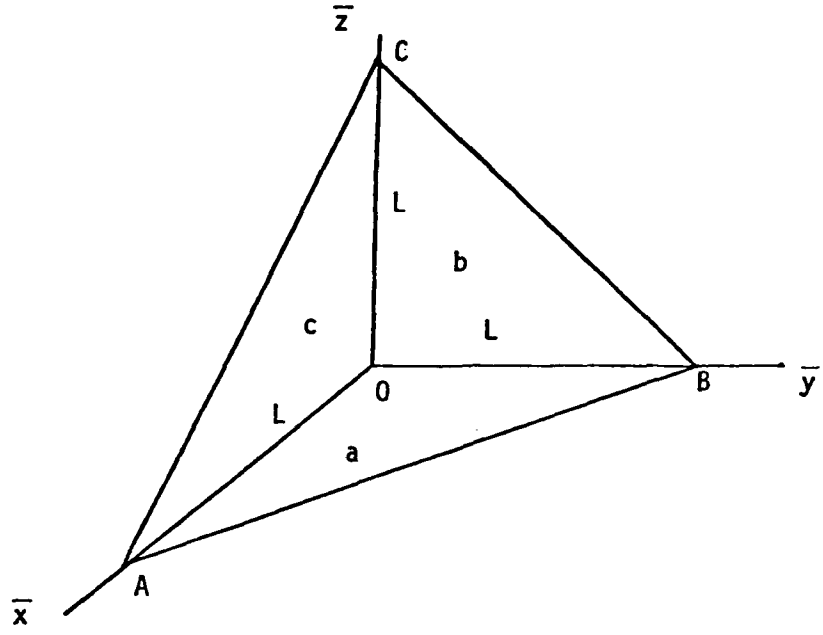

Fig. B-2. An Ideal Triangular Trihedral Corner Reflector

Thus, after bouncing off of three successive surfaces of the trihedral corner, the radiation (ray) is sent back directly toward the source - not too surprising a result.

For an ideal triangular or square trihedral corner reflector oriented as the one shown in Fig. B-2, the maximum backscatter (radar cross section) is realized for an incident ray having the following set of direction cosines,

$$\bar{I} = \left\{ -\frac{1}{\sqrt{3}}, -\frac{1}{\sqrt{3}}, -\frac{1}{\sqrt{3}} \right\} . \tag{B-25}$$

If surface a of Fig. (B-2) is rotated about its long edge $\overline{AB}$ by a small angular amount ε_{AB}, one can find the direction of the ray leaving the corner, by the same procedure just used for an ideal corner reflector. The resulting outgoing ray is

$$\bar{R} = (\alpha', \beta', \gamma'), \tag{B-26}$$

where

$$\alpha' = \frac{1}{\sqrt{3}} \cos 2\varepsilon_{AB} + \frac{1}{\sqrt{6}} \sin 2\varepsilon_{AB}$$

$$\beta' = \frac{1}{\sqrt{3}} \cos 2\varepsilon_{AB} + \frac{1}{\sqrt{6}} \sin 2\varepsilon_{AB}$$

$$\gamma' = \frac{1}{\sqrt{3}} \cos 2\varepsilon_{AB} - \frac{2}{\sqrt{6}} \sin 2\varepsilon_{AB}. \tag{B-26}$$

This outgoing ray is not oriented along the unit vector $\bar{Q}$ denoting the source location, which is given by

$$\bar{Q} = \left\{ \frac{1}{\sqrt{3}}, \frac{1}{\sqrt{3}}, \frac{1}{\sqrt{3}} \right\} . \tag{B-27}$$

The angular error δ_{AB} associated with the ray leaving the misaligned corner reflector can be formed by taking the dot product of $\overline{R}$ and $\overline{Q}$. Thus,

$$\overline{R} \cdot \overline{Q} = \cos\delta_{AB} = \cos 2\varepsilon_{AB} \ , \tag{B-28}$$

or

$$\boxed{\delta_{AB} = 2\varepsilon_{AB}} \ . \tag{B-29}$$

For a small rotation of surface a about $\overline{AB}$, one has a displacement of the surface $\overline{AOB}$ from the origin O by an amount λ/N such that to a good

$$\varepsilon_{AB} = \frac{\sqrt{2}\lambda}{L\ n} \ , \tag{B-30}$$

and so

$$\boxed{\delta_{AB} = \frac{2\sqrt{2}\lambda}{L\ n}} \ . \tag{B-31}$$

Before considering some other possible misalignments associated with trihedral corner reflectors, we note that Eq. (B-29) is also applicable to a dihedral corner which has one ot its surfaces rotated an angle ε_{AB} about the edge between its two surfaces. If each surface dimension normal to the intersecting edge is L, one has that

$$\varepsilon_{AB} = \frac{\lambda}{Ln} \tag{B-30'}$$

Here λ/n is the displacement of the far edge of a dihedral surface from its ideal (square) position. Combining Eqs. (B-29) and (B-30'), we have for the dihedral corner reflector that

$$\boxed{\delta_{AB} = \frac{2\lambda}{Ln}} \tag{B-31}$$

Let us next consider a trihedral corner reflector having its bottom surface a (i.e., the one normally in the x-y plane) rotated an angle ϵ_y about the y-axis. Thus,

$$\overline{N}_a = (\sin\epsilon_y, 0, \cos\epsilon_y). \tag{B-32}$$

Also let the incoming ray be oriented as it was before in Eq. (B-25).

Using the same ray tracing procedure that was demonstrated above, one finds that the outgoing ray $\overline{R}$ is given by

$$\overline{R} = (\alpha', \beta', \gamma'), \tag{B-33}$$

where

$$\alpha' = \frac{1}{\sqrt{3}} (\cos 2\varepsilon_y + \sin 2\varepsilon_y)$$

$$\beta' = \frac{1}{\sqrt{3}}$$

$$\gamma' = \frac{1}{\sqrt{3}} (\cos 2\varepsilon_y - \sin 2\varepsilon_y).$$

Substituting Eqs. (B-27) and (B-33) into (B-28), we find the outgoing ray has a directional error δ_y given by

$$\overline{R} \quad \overline{Q} = \cos\delta_y = \frac{1}{3} (1 + 2 \cos 2\varepsilon_y), \tag{B-34}$$

which can be rewritten as

$$\boxed{\sin \frac{\delta_y}{2} = \sqrt{\frac{2}{3}} \sin\varepsilon_y} \quad . \tag{B-35}$$

When $|\varepsilon_y| << 1$, we have to a good approximation that

$$\boxed{\delta_y = 2\sqrt{\frac{2}{3}}\, \varepsilon_y} \tag{B-36}$$

For a small rotation of surface a about the y-axis, the opposite corner of the surface has a small displacement from the ideal point A shown in Fig. B-2. To a good approximation this displacement is

$$\varepsilon_y = \frac{\lambda}{Ln} \quad . \tag{B-37}$$

Hence, we have approximately that

$$\boxed{\delta_y = 2\sqrt{\frac{2}{3}}\,\frac{\lambda}{Ln}} \quad . \tag{C-38}$$

The last case to be considered here is a trihedral corner with two surfaces misaligned. Let surface a of the trihedral corner be rotated by an amount ε_y about the y-axis as before. Also, let the surface c be rotated by an amount ε_z about the z-axis. Hence we have

$$\overline{N}_a = \left\{\sin\varepsilon_y,\ 0,\ \cos\varepsilon_y\right\} \tag{B-39}$$

and

$$\overline{N}_c = \left\{0,\ \cos\varepsilon_z,\ \sin\varepsilon_z\right\}. \tag{B-40}$$

Of course, we still have that the third surface is oriented such that

$$\overline{N}_b = (1,0,0) \tag{B-41}$$

and the source location is oriented so that

$$\overline{Q} = \left\{\frac{1}{\sqrt{3}}\ ,\ \frac{1}{\sqrt{3}}\ ,\ \frac{1}{\sqrt{3}}\right\} \quad . \tag{B-42}$$

Applying ray tracing techniques to a trihedral corner reflector with the above misalignments results in the following outgoing ray.

$$\overline{R} = \left\{\frac{1}{\sqrt{3}}\left[\left(\cos2\varepsilon_z + \sin2\varepsilon_z\right)\ \cos2\varepsilon_y + \sin2\varepsilon_y\right]\ ,\right.$$

$$\frac{1}{\sqrt{3}}\left(\cos2\varepsilon_z - \sin2\varepsilon_y\right)\ ,$$

$$\left.\frac{1}{\sqrt{3}}\left[\cos2\varepsilon_y - \left(\cos2\varepsilon_z + \sin2\varepsilon_z\right)\sin2\varepsilon_y\right]\right\} . \tag{B-43}$$

The dot product of $\overline{R}$ and $\overline{Q}$ yields the following expressions for the angular error δ_{y-z} associated with the outgoing ray.

$$\overline{R} \cdot \overline{Q} = \cos\delta_{y-z}$$

$$= \frac{1}{3}\left[\cos 2\varepsilon_y \left(1 + \cos 2\varepsilon_z + \sin 2\varepsilon_z\right) + \cos 2\varepsilon_z \right.$$

$$\left. + \sin 2\varepsilon_z \left(1 - \cos 2\varepsilon_z - \sin 2\varepsilon_z\right) - \sin 2\varepsilon_z \right] . \qquad \text{(B-44)}$$

If both surface misalignments are small (i.e., $|\varepsilon_y| \ll 1$ and $|\varepsilon_z| \ll 1$), the above result can be rewritten to a good approximation as

$$\boxed{\delta_{y-z} = 2\sqrt{\frac{2}{3}} \left(\varepsilon_y^2 + \varepsilon_y\varepsilon_z + \varepsilon_z^2\right)^{1/2}} \quad . \qquad \text{(B-45)}$$

Note that the magnitude of δ_{y-z} is dependent upon the relative senses of ε_y and ε_z. For example, if

$$\varepsilon_y = \varepsilon_z = \varepsilon \ , \qquad \text{(B-46)}$$

then

$$\boxed{\delta_{y-z} = 2\sqrt{2}\,\varepsilon} \quad . \qquad \text{(B-47)}$$

But if

$$\varepsilon_y = -\varepsilon_z = \hat{\varepsilon}, \qquad \text{(B-48)}$$

then

$$\boxed{\delta_{y-z} = 2\sqrt{\frac{2}{3}}\,\hat{\varepsilon}} \quad . \qquad \text{(B-49)}$$

which is identical to the result obtained when only one surface was rotated. (See Eq. (B-36).

Let us determine the reduction in radar cross section that results for the various corner misalignments considered above. For both the ideal triangular and square trihedral corner reflectors, the returning energy appears, in the far field, to be reflecting off of a regular hexagonal disk. For a triangular trihderal corner, an edge dimension of the regular hexagon is

$$e_T = \frac{\sqrt{2}}{3} L. \tag{B-50}$$

The corresponding edge dimension for a square trihedral corner, is

$$e_S = \sqrt{\frac{2}{3}} L. \tag{B-51}$$

To proceed without considerable difficulty, we assume that the radiation pattern associated with a hexagonal disk can be adequately represented by the pattern associated with a circular disk of equal area. The disk diameters corresponding to the effective apertures associated with triangular and square dihedral corner reflectors are

$$d_T = \frac{2}{\pi^{\frac{1}{2}} 3^{\frac{1}{4}}} L = 0.8574L, \tag{B-52}$$

and

$$d_S = 2 \frac{3^{\frac{1}{4}}}{\pi^{\frac{1}{2}}} L = 1.485L. \tag{B-53}$$

The normalized radar cross section $\hat{\sigma}$ for a circular disk of diameter d is

$$\hat{\sigma} = \left[2 \frac{J_1(\pi d\delta/\lambda)}{\lambda d\delta/\lambda} \right]^2 , \qquad \text{(B-54)}$$

where $J_1(\cdot)$ is the first-order Bessel function of the first kind and δ is pointing angle with respect to the surface normal. Note that the above expression is the Airy disk pattern associated with a uniformally-weighted circular aperture.

Equation (B-54) can be used to estimate the loss in monostatic radar cross section for either a misaligned triangular or square trihedral corner reflector. The parameter d must be replace by the expressions for d_T or d_S, respectively. Depending upon the type of misalignment, the angle δ must then be replaced by the appropriate expression for pointing error derived above - see Eqs. (B-29), (B-36), and (B-45).

By assuming that the argument of $J_1(\cdot)$ is on the order of $\sqrt{3}$ or less, the above expression for $\hat{\sigma}$ can be adequately represented by the first three terms of its Taylor series expansion. Thus, we have the following good approximation

$$\hat{\sigma} \quad 1 - \frac{1}{4} (\pi d\delta/\lambda)^2 + \frac{5}{192} (\pi d\delta/\lambda)^4 , \qquad \text{(B-55)}$$

for

$$\left(\frac{\pi d\delta}{\lambda} \right)^2 < 3 \qquad \text{(B-56)}$$

If the above equation for $\hat{\sigma}$ is rewritten in terms of the linear displacement λ/n of the edge or corner opposite the line of rotation, one obtains, in general, that

$$\boxed{\theta = 1 - \frac{p}{n^2} + \frac{q}{n^4}} \quad . \tag{B-57}$$

The coefficients, p and q, are tabulated in Table B-1 for the various misalignments that have been considered and for the two types (i.e., triangular or square) of trihedral reflector under consideration.

To obtain the coefficients, p and q, for the dihedral corner reflector, one must consider the radar cross section associated with a rectangular aperture. For an ideal dihedral reflector with one surface in the x-y plane, the maximum radar cross section is realized at an elevation angle of 45 deg. The normalized radar cross section as a function of the elevation angle δ from the maximum backscatter direction is

$$\theta = \left(\frac{\sin \pi \sqrt{2}\, L\delta/\lambda}{\pi \sqrt{2}\, L\delta/\lambda} \right)^2 \quad . \tag{B-58}$$

Approximating the above expression by the first three terms of its Taylor series expansion, we obtain

$$\theta = 1 - \frac{1}{3} (\pi \sqrt{2}\, L\delta/\lambda)^2 + \frac{2}{45} (\pi \sqrt{2}\, L\delta/\lambda)^4 \quad . \tag{B-59}$$

Substituting Eq. (B-31') into (B-59) to eliminate the L/λ, we obtain the p and q values listed in Table B-1 for the dihedral reflector. Thus, expression (B-57) for θ can be used for all the misalignments cases which we have considered. Using Eq. (B-57) and the p and q values given in Table B-1, we calculate specific misalignments which result in 1dB and

TABLE B-1

COEFFICIENTS FOR DETERMINING δ OF MISALIGNED CORNER REFLECTORS

Description of Reflector and Misalignment	p	q
TRIANGULAR TRIHEDRAL		
Rotation of 1 surface about its long edge	$8\pi/\sqrt{3} = 14.51$	$80\pi^2/9 = 87.73$
Rotation of 1 surface about a short edge	$8\pi/3\sqrt{3} = 4.837$	$80\pi^2/81 = 9.748$
Equal, Positive Rotations of 2 surfaces about any two of their short edges	$8\pi\ \sqrt{3} = 14.51$	$80\pi^2/9 = 87.73$
SQUARE TRIHEDRAL		
Rotation of 1 surface about its diagonal	$8\pi\sqrt{3} = 43.53$	$80\pi^2 = 789.6$
Rotation of 1 surface about one of its edges	$8\pi/\sqrt{3} = 14.51$	$80\pi^2/9 = 87.73$
Equal, Positive Rotation of 2 surfaces about any two of their edges	$8\pi\sqrt{3} = 43.53$	$80\pi^2 = 789.6$
SQUARE DIHEDRAL		
Rotation of one surface about the common edge	$8\pi^2/3 = 26.32$	$128\pi^4/45 = 277.1$

3dB loss in radar cross section. The results of this exercise are presented in Table B-2. This table clearly demonstrates the difficulty associated with constructing calibrated corner reflectors. If the radar cross section associated with a common triangular trihedral reflector is to be within 1dB of its theoretical value, the linear displacements of one corner surface must be limited to $\lambda/4.6$ or $\lambda/8$, depending upon the specific type of misalignment. At x-band wavelengths, these tolerance dimensions correspond to 0.26 in. and 0.15 in. over the extent of the surface involved. For a square trihedral corner the alignment requirements are roughtly a fact of two smaller. If a dihedral corner reflector is to have a radar cross section which is within 1dB of its theoretical value, it must be aligned to $\lambda/11$ over the extent of a surface. At x-band, this tolerance is roughly 0.11 in.

As a final reminder, note that only the effects of misaligned corner reflector surfaces have been considered. Additional degradation in radar cross section will also result from actual surfaces not being perfectly flat. One expects that the tolerance on bowing and sagging surfaces should be of the same order of magnitude as the tolerances listed in Table B-2 for misaligned surfaces.

TABLE B-2

CORNER REFLECTOR MISALIGNMENTS CORRESPONDING TO 1dB AND 3dB LOSSES IN RADAR CROSS SECTION

Description of Reflector and Misalignment	Displacements Resulting in 1dB Loss	Displacements Resulting in 3dB Loss
TRIANGULAR TRIHEDRAL		
Rotation of one surface about its long edge	λ/8.0	λ/4.5
Rotation of one surface about a short edge	λ/4.6	λ/2.6
Equal, Positive Rotations of two surfaces about any two of their short edges	λ/8.0	λ/4.5
SQUARE TRIHEDRAL		
Rotation of one surface about its diagonal	λ/13.8	λ/7.9
Rotation of one surface about a common edge	λ/8.0	λ/4.5
Equal, Positive Rotation of two surfaces about any two of their edges	λ/13.8	λ/7.9
SQUARE DIHEDRAL		
Rotation of one surface about the common edge	λ/10.8	λ/6.2

APPENDIX C

RECONSTRUCTION OF DIGITAL SAR DATA

A large number of computer simulations have been developed at SAI/Tucson which consider the reconstruction of digital SAR data. Optimum Gaussian interpolators [1, 2], the effects of up-sampling [3, 4], and spectrum analysis [1, 5, 6], to name a few. The majority of the analysis makes use of a two-dimensional Gaussian filter to reconstruct the digital SAR data. The Gaussian filter is an excellent image reconstructor for digital SAR data. In addition, this filter often can be used to approximate the cross section of writing beams used in softcopy and hardcopy displays (e.g., LBR's and CRT's).

To obtain the resultant imagery at the display, the digital SAR data is convolved with a Gaussian filter. For the one-dimensional case it can be written as

$$\hat{f}(x) = \sum_{k=-\infty}^{\infty} f(kT_x)\, e^{-\left((x-kT_x)^2/2\sigma^2\right)}$$

where

T_x is the sampling interval,

$f(kT)$ are the discrete digital SAR data,

σ is the Gaussian spot size, and

$\hat{f}(x)$ is the interpolated or reconstructed output.

From previous analysis [1], the optimum Gaussian spot size has been found to be approximately 60% of the sampling interval, which can be written as

$$\sigma = 0.6T \ .$$

This optimum spot size value was found by comparing the reconstructed point target with the ideal impulse response of the digital SAR processor. A typical reconstructed point target is illustrated in Figure C-1. In this figure, the sampling rate is at 1.25 x Nyquist[1], the returns are cosine weighted and the resulting image digital data are power-law compressed to the 0.3 power prior to applying the Gaussian filter. The sampling shift is assumed to be 0% (i.e., the peak of the impulse response is sampled). The continuous curve represents the ideal impulse response to a point target and the non-continuous curve represents the interpolated (filtered) sampled impulse response.

From plots like Fig. C-1, the IPR width and peak sidelobe level can be measured. Given the digital SAR data from the output of the FTB processor a similar analysis can be performed. The two-dimensional digital SAR data is convolved with a two-dimensional Gaussian digital filter yielding,

$$\hat{f}(x,y) = \sum_{k=-\infty}^{\infty} \sum_{\ell=-\infty}^{\infty} f(kT_x, \ell T_y)\, e^{-\left[\left((x-kT_x)^2/2\sigma_x^2\right) + \left((y-\ell T_y)^2/2\sigma_y^2\right)\right]}.$$

From the resultant imagery, $\hat{f}(x,y)$, the image quality parameters can be measured. Namely, the IPR width, peak side lobe level, contrast ratio, intermodulation distortion, etc.

---

[1]The Nyquist rate is defined to be the minimum sampling rate at the inphase and quadrature outputs of the SAR processor before experiencing the effects of spectral folding or aliasing.

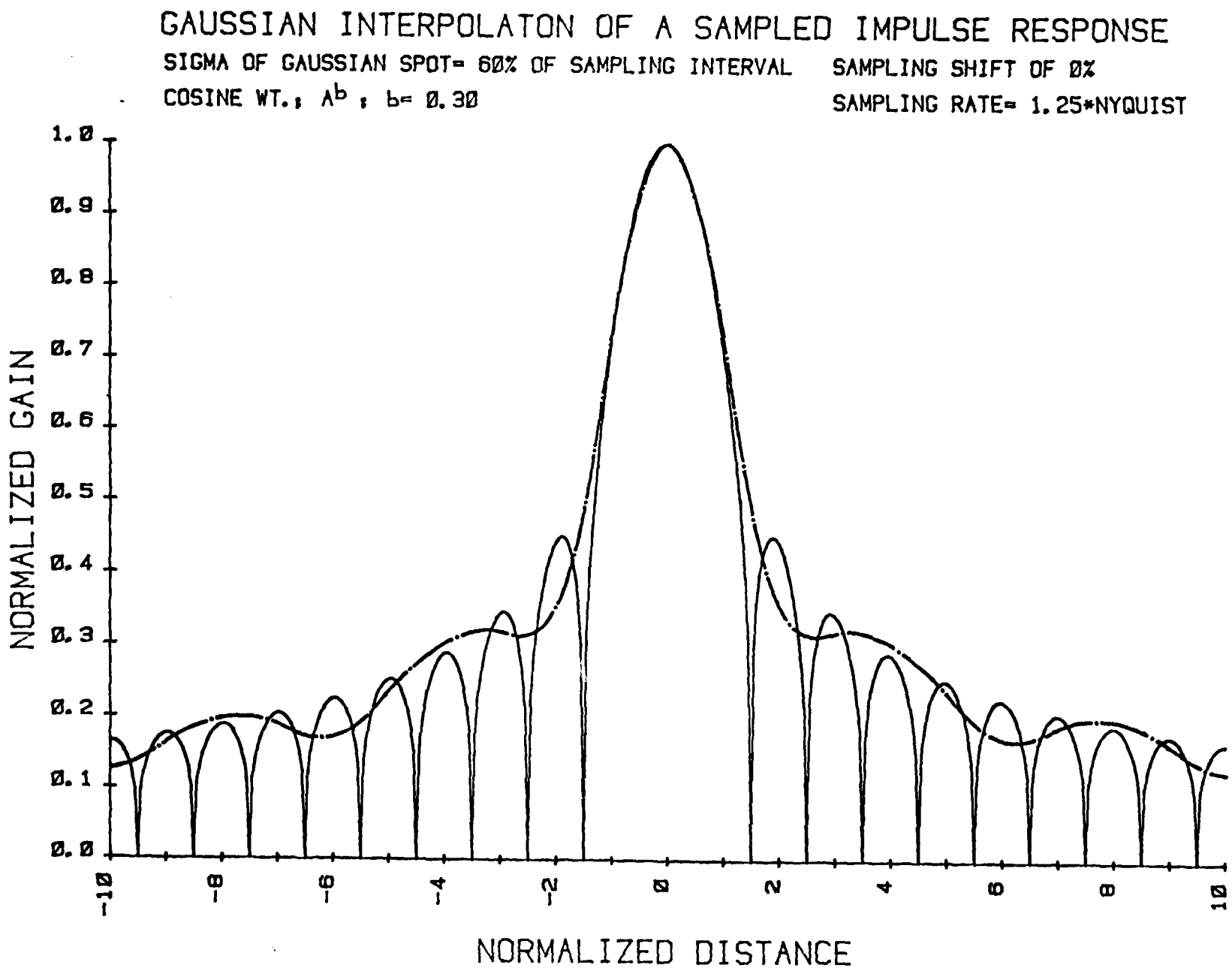

Fig. C-1 Typical Reconstructed Point Target.

SECURITY CLASSIFICATION OF THIS PAGE (When Data Entered)

REPORT DOCUMENTATION PAGE		READ INSTRUCTIONS BEFORE COMPLETING FORM
1. REPORT NUMBER	2. GOVT ACCESSION NO. AD-A084400	3. RECIPIENT'S CATALOG NUMBER
4. TITLE (and Subtitle) RADAR TEST RANGE DESIGN CONSIDERATIONS		5. TYPE OF REPORT & PERIOD COVERED FINAL
		6. PERFORMING ORG. REPORT NUMBER TR-04-165-3
7. AUTHOR(s) DINO SOFIANOS		8. CONTRACT OR GRANT NUMBER(s) F33657-79-C-0178
9. PERFORMING ORGANIZATION NAME AND ADDRESS Science Applications, Inc., Suite A-214 5055 E. Broadway, Tucson, AZ 85711		10. PROGRAM ELEMENT, PROJECT, TASK AREA & WORK UNIT NUMBERS
11. CONTROLLING OFFICE NAME AND ADDRESS Aeronautical Systems Division UPD-X Program Office (AERW) WPAFB, Ohio		12. REPORT DATE 29 April 1980
		13. NUMBER OF PAGES
14. MONITORING AGENCY NAME & ADDRESS(if different from Controlling Office)		15. SECURITY CLASS. (of this report) Unclassified
		15a. DECLASSIFICATION/DOWNGRADING SCHEDULE

16. DISTRIBUTION STATEMENT (of this Report)

Approved for public release, distribution unlimited.
Copies of this document may be obtained from the Defense Documentation Center, Cameron Station, Alexandria, VA 22314

17. DISTRIBUTION STATEMENT (of the abstract entered in Block 20, if different from Report)

18. SUPPLEMENTARY NOTES

19. KEY WORDS (Continue on reverse side if necessary and identify by block number)

1 Radar Performance
2 Radar System Performance
3 Synthetic Aperture Radar (SAR)
Side Looking Radar
Mapping Radar
4 Ranges (Facilities)
5 Radar Equipment Reflectors

20. ABSTRACT (Continue on reverse side if necessary and identify by block number)

This report presents considerations for and the preliminary design of a synthetic aperture RADAR (SAR) test range.

DD FORM 1 JAN 73 1473 EDITION OF 1 NOV 65 IS OBSOLETE

SECURITY CLASSIFICATION OF THIS PAGE (When Data Entered)